The Migrating Speed of Alternate Bars

Michihide Ishihara[1], **Hiroyasu Yasuda**[2]

[1]Graduate School of Science and Technology, Niigata University, Niigata, Japan
[2]Research Institute for Natural Hazards & Disaster Recovery Niigata University, Niigata, Japan

Key Points:

- The spatial distribution of the migrating speed of alternate bars that occur in rivers was determined.
- A hyperbolic partial differential equation for the bed level and migrating speed formula were derived.
- The most dominant physical quantity of migrating speed of alternate bars is the energy slope.

Corresponding author: Hiroyasu Yasuda, hiro@gs.niigata-u.ac.jp

Abstract

Alternate bars can spontaneously occur and develop in rivers. They are considered to be a wave phenomenon due to their geometrical features and propagation characteristics. Presently, there is insufficient knowledge about their propagation, which is an important wave phenomenon property. In this study, a flume experiment was conducted under the condition that alternate bars occur and develop. This investigation aims to understand the existence and the scale of migrating speed of these alternate bars. The bed and water levels during the occurrence and development of the alternate bars were measured frequently with a high spatial resolution. By comparing the geometrical changes in the bed shape, the migrating speed of the alternate bars has a spatial distribution that changes with time. To quantify the spatial distribution of the migrating speed of the alternate bars, a hyperbolic partial differential equation for the bed level and migrating speed formula were derived. A comparison of the measured values for the flume experiment showed that the derived formula is applicable. Using the formula of the migrating speed in this hyperbolic partial differential equation, the migrating speed was verified to have a spatial distribution. In addition, the distribution changes with the development of the alternate bars over time. This study demonstrates that the dominant physical quantity of the migrating speed is the energy slope from the experimental results and the migrating speed formula.

1 Introduction

Periodic forms can spontaneously form along a river channel's bed surface. These forms are called riverbed waves because of their geometrical shapes and physical properties. Riverbed waves can be classified as small-scale, mesoscale, and large-scale based on spatial scales, which include the wavelength and wave height (Seminara, 2010). Small-scale riverbed waves have wavelengths on the scale of the water depth; meso-scale riverbed waves have wavelengths on the river width scale and wave heights on the water depth scale. Large-scale riverbed waves have larger scales. The target of this study is alternate bars that correspond to meso-scale riverbed waves. Alternate bars are riverbed waves that spontaneously form in rivers. They are located in sites from the alluvial fan to the natural embankment. When observing alternate bars from the sky with aerial photographs, the tip part is diagonally connected to the left and right riverbanks; a deep-water pool is located on the downstream side of this tip. In addition, it is known that the phase of the alternate bars propagates in the same way as the water surface waves during flooding.

Over the years, many studies have been conducted on alternate bars. One of the initial studies consisted of the flume experiments that were performed by Kinoshita (Ryosaku, 1961). Kinoshita conducted long-term flume experiment to understand the dynamics of the alternate bars that can produce meandering streams. According to this experiment experiments, he reported that 1) alternate bars have a globally uniform migrating speed and wavelength, 2) alternate bars in the early stages of development have short wavelengths and fast migrating speeds, and 3) the migrating speed becomes slower with the development of wavelengths. These results have been confirmed in subsequent studies(Ikeda, 1983; Fujita & Muramoto, 1985; Nobuhisa et al., 1999). In addition to the aforementioned conclusions, he proposed a formula to calculate the migration speed of the alternate bars based on the experimental results, with the Froude number and shear velocity as the dominant physical quantities. However, the validity of this formula has not been demonstrated in the same study.

Besides studies using flume experiments, several studies have applied mathematical analyses to understand the alternate bar phenomenon. Perhaps the first

mathematical study on alternate bars was that performed by Callander (Callander, 1969). He extended the stability analysis of Kennedy (Kennedy, 1963) for small-scale bed waves to a two-dimensional plane problem and theoretically discussed the physical quantities that govern the generation of meso-scale riverbed waves. This study was the starting point for the research that aimed at predicting the conditions under which alternate bars occur and the wavelength and wave height of the alternate bars after development(Kuroki & Kishi, 1984; Colombini et al., 1987; Colombini & Tubino, 1991; Tubino, 1991; Doelman et al., 1993). When considering the literature that used these stability analyses, the studies by Callander (Callander, 1969) and Kuroki (Kuroki & Kishi, 1984) are important. They derived a formula to calculate the migrating speed corresponding to the wave number that maximizes the time amplification factor. The dominant physical quantities in the formula were the Froude number, Shields number (shear velocity), bed slope, and wave number. Moreover, in both the aforementioned studies, the value of the formula is compared with the measured value. It has been reported that the reproducibility of the formula to calculate the migrating speed is good.

With the rise of stability analysis, numerical analyses of the riverbed fluctuations during the occurrence and development of alternate bars began to be carried out. Shimizu et al. (Shimizu & Itakura, 1989) reported for the first time that numerical analysis can satisfactorily reproduce each process of the occurrence and the development of alternate bars. In recent years, Federici et al. (Federici & Seminara, 2003) reported the propagation direction of the riverbed waves by performing stability and numerical analyses.

Recent studies that have used flume experiments (Lanzoni, 2000a, 2000b; Miwa et al., 2007; Crosato et al., 2011, 2012; Venditti et al., 2012; Podolak & Wilcock, 2013) have investigated the effects of external factors such as the amount of sediment supply on the dynamics of the alternate bars. Crosato et al. (Crosato et al., 2011, 2012) reported that alternate bars eventually shift from being migrating bars to steady bars; they performed flume experiments and a numerical analysis to verify this. Next, Venditti et al. (Venditti et al., 2012) reported that when the sediment supply was interrupted after alternate bars occurred, the bed slope and shear stress decreased, and the bars disappeared accordingly. Podolak et al. (Podolak & Wilcock, 2013) also studied the response of alternate bars to sediment supply by increasing the sediment supply during the occurrence and development of alternate bars. It was demonstrated that a non-migrating bar changed to a migrating bar with an increase in the bed slope and shear stress owing to increase in the sediment supply. In addition, Eekhout et al.(Eekhout et al., 2013) investigated the dynamics of alternate bars in rivers for nearly three years and reported that the migrating speed decreased as the wavelength and wave height of the alternate bars increased and the bed slope decreased.

Thus far, the geometrical shape and physical properties of the alternate bars have been investigated. Based on the previous studies, it is possible to predict the presence or absence of the alternate bars and their geometric shapes to some extent. However, there is very little understanding of the nature of the migration speed of the alternate bars. Therefore, in this study, we focused on the migration speed while focusing on the physics of alternate bars. As this is not well understood, we carried out the following to clarify the existence and scale of the spatial distribution. Section 2 describes the outline of the flume experiment that uses the Stream Tomography (ST) method, which can simultaneously measure the geometric shapes of the water surface and the bed surface with a high spatial resolution; the results are also described. In Section 3, we assumed that the alternate bars can be regarded as a wave phenomenon, and we derived a hyperbolic partial differential equation (HPDE) for the bed level. In this study, the advection velocity that is given to the advection

term of the HPDE was used to calculate the migration speed of the alternate bars. In Section 4, the validity of the calculation formula that was derived in Section 3 was verified based on the characteristics of the HPDE and the measured values of the bed level that was obtained in Section 2. In Section 5, the spatial distribution of the migration speed of the alternate bars is quantified using the formula to calculate the migration speed. Section 6 describes the results that were obtained in Section 5, and Section 7 summarizes the research results.

2 Quantification of the Propagation Phenomenon in Alternate Bars based on the Flume Experiment

2.1 Experimental Setup

Figure 2 shows the plan view of the experiment flume. The experimental channel consisted of a flume channel with a straight rectangular cross section. The flume had a length of 12.0 m, a width of 0.45 m, and a depth of 0.15 m. Fixed weirs with the same width as the flume were located 2.0 m from the upstream and downstream ends of the flume. Over the section between 2.0 m and 10.0 m from the upstream end that was sandwiched by these weirs, the initial bed of the channel for the experiment was a set flat bed. The bed was composed of a non-cohesive material with a mean diameter of 0.76 mm and had a thickness of 5.0 cm.

For the water supply to the channel, circulation-type pumping from a water tank at the downstream end to a water tank at the upstream end was adopted; the water was steadily supplied. The accuracy of the water discharge was confirmed using an electromagnetic flowmeter.

2.2 Experimental Condition

The purpose of this study is to understand the existence and scale of the spatial distribution of the migration speed of the alternate bars. An alternate bar is a typical bed wave in a river that is attributed from an alluvial fan to a natural embankment.

Therefore, in the following experiments, we set the hydraulic conditions in which the alternate bars developed. It has been theoretically shown that the occurrence of alternate bars can be estimated using the river width depth ratio. Therefore, in this study, we set $BI_0^{0.2}/h_0$ to 13.5, which corresponds to the occurrence area of the alternate bars in the area division map as shown by Kuroki and Kichi(Kuroki & Kishi, 1984). B is channel width, I_0 is the initial uniform bed slope, h_o is the initial uniform water depth. The bed slope of the flume is 1/160, the water discharge is 1.5 L/s, the flow velocity and water depth are 0.28 m/s and 0.012 m, respectively, on the initial flat bed. The Shields number during the initial condition is 0.06, which is higher than the critical Shields number (0.034) that was obtained from Iwagaki's formula (Yuichi, 1956). The sediment supply along the upstream end was not provided. This is because by comparing the effect of the sediment supply with and without a preliminary experiment, it was observed that the spatial distribution of the migrating speed of alternate bars and its temporal changes occurred without the sediment supply.

The water flow was carried out for 4 h during this experiment with the aforementioned conditions. At this time, alternate bars developed, and its propagation and shape change became slow.

2.3 Measurement Method for the Bed Surface and Water Surface

In this study, we used ST, which was developed by Hoshino et al., to measure the bed level and water level in a plane while the water is flowing. For details on the principles of the ST measurement, refer to Appendix A. In this study, the aforementioned measurements were performed with a spatial resolution of 2 cm^2 for every minute. The water depth was calculated from the difference between the water level and bed level. The water surface slope was calculated from the central spatial difference between the water levels.

2.4 Measurement Results

This section explains the propagation phenomenon of alternate bars using Fig. 3 and Fig. 4 based on the results of the high spatial resolution that was measured by ST.

Figure 3 shows the plan view of the deviation of the bed level by ST. The origin of the vertical coordinate of the ST is the flume bottom. Therefore, the water level and bed level represent the height from the bed of the flume. In this study, we measured the bed level at 1-minute intervals using ST. However, the results at 20-minute intervals indicate that a clear change can be easily confirmed under the set of hydraulic conditions that are shown. In this study, the initial bed surface was created so that it was as flat as possible. However, it was difficult to obtain a perfectly flat bed due to the accuracy limit of the bed surface that shapes the setup. It has been confirmed that the alternate bars, which occurred and developed under the aforementioned initial conditions, are almost the same as that developed in previous studies (Ryosaku, 1958; Federici & Seminara, 2003; Crosato et al., 2011; Venditti et al., 2012; Podolak & Wilcock, 2013).

First, the bed shape did not change from the flat bed as the initial condition (Fig. 3(a),(b)). Second, it was possible to see the bed topography in which the deposition and scouring are alternately repeated in the downstream direction, that is 1.0 m, 2.5 m, and 4.0 m from the upstream end; thus, it was possible to confirm that the alternate bars occurred (Fig. 3(c)). In this study, we defined 40 min, in which the geometric features of the alternate bars were confirmed from the measured result by the ST, as the occurrence time of the alternate bars. The alternate bars developed the topography over time; they were deposited more on the riffle side and scoured more on the pool. Subsequently, the entire alternate bars moved gradually in the downstream direction. The development and propagation of the alternate bars was significant from 40 min to 140 min (Fig. 3(c) to (h)). However, there was minimal development or propagation after 140 min (Fig. 3 (h) to (m)). From this result, comparing the migrating speed of the alternate bars during the early stage of development with the migrating speed of the fully developed alternate bars, it can be observed that the migrating speed in the former state is faster and the in latter is slower. Figure 4 shows the longitudinal distribution of the deviation in the bed level on the green dotted line in Fig. 3. Figure 4 shows (a) the initial stage of the experiment, (b) the occurrence of the alternate bars, (c) the intermediate stage of the experiment, and (d) the final stage of the experiment. Figure 4 shows three results, where each one is 20 min apart. First, the deviation of the bed level was confirmed to maintain a nearly flat bed from 1 min to 20 min (Fig. 4(a)). After (b) 40 min, two bed undulations developed that were 1.5 m and 4.0 m from the upstream end. The bed undulations developed their amplitudes and propagated in the downstream direction. As a result, ST was confirmed to observe the wave nature of the alternate bars.

The linear wave theory indicates that the phase propagates without deforming the waveform if a wave propagates with a spatial and temporal constant migrating

speed. Conversely, in the nonlinear wave theory, in which the migrating speed has a spatial distribution and temporal changes, the wave propagates with deformation of the waveform. From the viewpoint of the aforementioned wave theories, it is inferred that the migrating speed of the alternate bars at the time of the occurrence of the alternate bars in (b) has a spatial distribution; it changes with time and has nonlinear wave properties. Conversely, in (c) the intermediate stage of the experiment and (d) the final stage of the experiment, there was no deformation of the waveform and propagation. Thus, it was inferred that the migrating speed was almost zero; moreover, it is presumed that the wave nature was lost (Fig. 4(c),(d)).

3 Derivation of the Calculation Formula for the Migrating Speed of the Alternate Bars

As shown in the previous section, the measurement results of this study show the wave nature in the process of the occurrence and development of the alternate bars. These findings are similar to what has been reported in the literature (Ryosaku, 1958; Federici & Seminara, 2003; Crosato et al., 2011; Venditti et al., 2012; Podolak & Wilcock, 2013). In other words, there is scope for quantifying the spatial distribution of the migration speed by an indirect method that uses a mathematical model such as the HPDE(Fujita et al., 1985), which is suitable for describing the wave phenomena. The formula for calculating the migration speed is also derived from the stability analysis (Callander, 1969; Kuroki & Kishi, 1984). However, because the formula calculates the migrating speed for each wave number, the spatial distribution of the migrating speed cannot be quantified. Therefore, in this study, we can use the HPDE for the bed level z and quantify the spatial distribution of the migration speed of the alternate bars using the advection velocity of the advection term that has the same formula.

This section describes the derivation process of the HPDE for the bed level z. In addition, four different formulas can be obtained depending on the physical assumptions. This includes whether the dimension is one-dimensional or two-dimensional, and whether the flow is stationary or unsteady. First, regarding the stationarity of the flow, as it was confirmed that the non-stationary state in the phenomenon targeted by this study is very small from the verification results that are described in Appendix B, we decided to deal only with the stationary state. In terms of the dimensions, the geometric shape of the alternate bars and the flow there each has two-dimensional plane characteristics. Therefore, we decided to derive a two-dimensional stationary equation. The derivation of the HPDE for the bed level can be used for the continuous equation of the sediment, sediment functions, and the equation of the water surface profile. For the derivation, the Exner equation was used as the continuous equation of the sediment, and the Meyer–Peter and Müller (M.P.M) formula was used as the sediment function and the two-dimensional equation of the water surface profile. The application of the HPDE to the various sediment functions was examined using a method that is described in the next section. In this study, the M.P.M formula, which is simple and has good applicability, was adopted. Vectors for the longitudinal Eq. (2) and transverse Eq. (3) for the sediment flux are assumed to match the flows. Equation (6) was used to calculate the Shields number. Above all, we derived the steady two-dimensional equation of the water surface profile (Eq. (4), Eq. (5)) to derive the HPDE for the bed level. For the details on the derivation process of the steady two-dimensional equation for the water surface profile, please refer to Appendix C.

$$\frac{\partial z}{\partial t} + \frac{1}{1-\lambda}\left(\frac{\partial q_{Bx}}{\partial x} + \frac{\partial q_{By}}{\partial y}\right) = 0 \tag{1}$$

$$q_{Bx} = 8(\tau_* - \tau_{*c})^{3/2}\sqrt{sgd^3}\,\frac{u}{V} \tag{2}$$

$$q_{By} = 8(\tau_* - \tau_{*c})^{3/2}\sqrt{sgd^3}\frac{v}{V} \tag{3}$$

$$\begin{aligned}\frac{\partial h}{\partial x} = &-\frac{\partial z}{\partial x} - I_{ex} - \frac{3}{10}\frac{u^2}{gI_{ex}}\frac{\partial I_{ex}}{\partial x} \\ &+\frac{1}{5}\frac{uv}{gI_{ey}}\frac{\partial I_{ey}}{\partial y} - \frac{1}{2}\frac{uv}{gI_{ex}}\frac{\partial I_{ex}}{\partial y}\end{aligned} \tag{4}$$

$$\begin{aligned}\frac{\partial h}{\partial y} = &-\frac{\partial z}{\partial y} - I_{ey} - \frac{3}{10}\frac{v^2}{gI_{ey}}\frac{\partial I_{ey}}{\partial y} \\ &-\frac{1}{2}\frac{uv}{gI_{ey}}\frac{\partial I_{ey}}{\partial x} + \frac{1}{5}\frac{uv}{gI_{ex}}\frac{\partial I_{ex}}{\partial x}\end{aligned} \tag{5}$$

$$\tau_* = \frac{hI_e}{sd} \tag{6}$$

where: z is the bed level, t is the time, λ is the porosity of the bed, q_{Bx} is the longitudinal sediment flux, x is the distance of the longitudinal direction, q_{By} is the transverse sediment flux, y is the distance of the transverse direction, τ_* is the composite Shields number, τ_{*c} is the critical Shields number, s is the specific gravity of the sediments in water, g is the gravity acceleration, d is the sediment size, u is the longitudinal flow velocity, V is the composite flow velocity, v is the transverse of the flow velocity, and h is the depth. In addition, $I_{bx} = -\partial z/\partial x$ is the longitudinal bed slope, I_{ex} is the longitudinal energy slope, $I_{by} = -\partial z/\partial y$ is the transverse bed slope, I_{ey} is the transverse energy slope, and n is the coefficient of roughness.

First, by applying the chain rule of differentiation to $\partial q_{Bx}/\partial x$ in Eq. (1), we obtain the following.

$$\begin{aligned}\frac{\partial q_{Bx}}{\partial x} &= \frac{\partial q_{Bx}}{\partial \tau_*}\left(\frac{\partial \tau_*}{\partial h}\frac{\partial h}{\partial x} + \frac{\partial \tau_*}{\partial I_e}\frac{\partial I_e}{\partial x}\right) \\ &= \frac{\partial q_{Bx}}{\partial \tau_*}\left(\frac{I_e}{sd}\frac{\partial h}{\partial x} + \frac{h}{sd}\frac{\partial I_e}{\partial x}\right) \\ &= \frac{\partial q_{Bx}}{\partial \tau_*}\frac{I_e}{sd}\left(\frac{\partial h}{\partial x} + \frac{h}{I_e}\frac{\partial I_e}{\partial x}\right)\end{aligned} \tag{7}$$

In addition, $\partial I_e/\partial x$ in Eq. (7) becomes the following due to the application of the chain rule to differentiate the Manning flow velocity Eq. (8).

$$V = \frac{1}{n}{I_e}^{1/2}h^{2/3} \tag{8}$$

$$\frac{\partial I_e}{\partial x} = \frac{\partial I_e}{\partial h}\frac{\partial h}{\partial x} + \frac{\partial I_e}{\partial V}\frac{\partial V}{\partial x} = -\frac{4}{3}\frac{I_e}{h}\frac{\partial h}{\partial x} + 2\frac{I_e}{V}\frac{\partial V}{\partial x} \tag{9}$$

Substituting Eq. (9) in Eq. (7) and rearranging this, we can obtain the following equation.

$$\frac{\partial q_{Bx}}{\partial x} = \frac{\partial q_{Bx}}{\partial \tau_*}\frac{I_e}{sd}\left(-\frac{1}{3}\frac{\partial h}{\partial x} + 2\frac{h}{V}\frac{\partial V}{\partial x}\right) \tag{10}$$

$\partial q_{Bx}/\partial \tau_*$ in the aforementioned equation is as follows.

$$\frac{\partial q_{Bx}}{\partial \tau_*} = 12(\tau_* - \tau_{*c})^{1/2}\sqrt{sgd^3}\left(\frac{u}{V}\right) \tag{11}$$

Equation (4) is used for $\partial h/\partial x$. Substituting Eq. (4) and Eq. (11) in Eq. (10), Eq. (10) is as follows.

$$\begin{aligned}\frac{\partial q_{Bx}}{\partial x} = &4(\tau_* - \tau_{*c})^{1/2}\sqrt{sgd^3}\left(\frac{u}{V}\right)\frac{I_e}{sd}\Big(\frac{\partial z}{\partial x} + I_{ex} \\ &+\frac{3}{10}\frac{u^2}{gI_{ex}}\frac{\partial I_{ex}}{\partial x} - \frac{1}{5}\frac{uv}{gI_{ey}}\frac{\partial I_{ey}}{\partial y} + \frac{1}{2}\frac{uv}{gI_{ex}}\frac{\partial I_{ex}}{\partial y} + 6\frac{h}{V}\frac{\partial V}{\partial x}\Big)\end{aligned} \tag{12}$$

In addition, $\partial q_{By}/\partial y$ is arranged in the same process as Eq. (12), and the following equation is derived.

$$\frac{\partial q_{By}}{\partial y} = 4(\tau_* - \tau_{*c})^{1/2}\sqrt{sgd^3}\left(\frac{v}{V}\right)\frac{I_e}{sd}\left(\frac{\partial z}{\partial y} + I_{ey} + \frac{3}{10}\frac{v^2}{gI_{ey}}\frac{\partial I_{ey}}{\partial y} - \frac{1}{5}\frac{uv}{gI_{ex}}\frac{\partial I_{ex}}{\partial x} + \frac{1}{2}\frac{uv}{gI_{ey}}\frac{\partial I_{ey}}{\partial x} + 6\frac{h}{V}\frac{\partial V}{\partial y}\right) \tag{13}$$

By substituting Eq. (12) and Eq. (13) in Eq. (1), the following HPDE for the bed level z is derived.

$$\frac{\partial z}{\partial t} + M_x\frac{\partial z}{\partial x} + M_x I_{ex} + M_x F_x + M_y\frac{\partial z}{\partial y} + M_y I_{ey} + M_y F_y = 0 \tag{14}$$

In the aforementioned equation, M_x is the advection velocity of the longitudinal component of the bed level z. It is assumed to be closely related to the migration speed of the longitudinal component of the alternate bars, which is the subject of this study. M_y is the transverse migration speed of the alternate bars. M_x and M_y are not velocities of the sediments; they are supposed to be the propagation velocities of the bed level z. M_x and M_y are as follows.

$$M_x = \frac{4(\tau_* - \tau_{*c})^{1/2}\sqrt{sgd^3}\left(\frac{u}{V}\right)I_e}{sd(1-\lambda)} \tag{15}$$

$$M_y = \frac{4(\tau_* - \tau_{*c})^{1/2}\sqrt{sgd^3}\left(\frac{v}{V}\right)I_e}{sd(1-\lambda)} \tag{16}$$

From Eq. (15) and Eq. (16), it can be observed that the dominant physical quantities of the migrating speed are I_e and τ_*. In addition, F_x and F_y are as follows.

$$F_x = \frac{3}{10}\frac{u^2}{gI_{ex}}\frac{\partial I_{ex}}{\partial x} - \frac{1}{5}\frac{uv}{gI_{ey}}\frac{\partial I_{ey}}{\partial y} + \frac{1}{2}\frac{uv}{gI_{ex}}\frac{\partial I_{ex}}{\partial y} + 6\frac{h}{V}\frac{\partial V}{\partial x} \tag{17}$$

$$F_y = \frac{3}{10}\frac{v^2}{gI_{ey}}\frac{\partial I_{ey}}{\partial y} - \frac{1}{5}\frac{uv}{gI_{ex}}\frac{\partial I_{ex}}{\partial x} + \frac{1}{2}\frac{uv}{gI_{ey}}\frac{\partial I_{ey}}{\partial x} + 6\frac{h}{V}\frac{\partial V}{\partial y} \tag{18}$$

4 Verifying the Applications of the HPDE for the Bed Level z and the Migrating Speed Formula based on the Measured Values

This section verifies the applicability of the HPDE for the bed level z and the formula for the migrating speed, which was described in the previous section. Verification is achieved using the values of the ST and hydraulic analysis.

4.1 Hydraulics required to verify applicability

This section describes the hydraulic quantities that are required to verify the applicability of the HPDE and the calculation formula for the migrating speed, as explained in the next section. As demonstrated from the HPDE and the calculation formula of the migrating speed shown in the previous section, the hydraulic quantities that are required for the verification of the applicability are the water depth, energy slope, and flow velocity. The water depth can be obtained from the bed level and water level that is measured by the ST. However, the flow velocity and energy slope that are paired with the water depth have not been measured; this measurement is generally difficult. Therefore, we determined the flow velocity and energy slope by performing a numerical analysis.

For the numerical analysis, Nays2D included in iRIC (http://www.i-ric.org) can solve the two-dimensional plane hydraulic analysis. It was conducted with a bed level that was measured by the ST as a fixed bed.

The arrangement interval of the calculation points was 2 cm, which is the same as the resolution of the ST in the transverse and longitudinal directions. The upstream end boundary condition had a flow rate of 1.5 L $/s$; the downstream end boundary condition provided the measured water depth. In addition, the roughness coefficient was adjusted each time so that the calculated and measured values of the water depth matched and they were uniform over the entire section. Figure 5 shows the measured water depth. Figure 6 shows the difference between the measured water depth and the calculated value, which is dimensionless Δh_*. In addition, Fig. 7 illustrates the calculated flow velocity. Of these, Δh_* represents the calculation accuracy of the numerical analysis. By focusing on Δh_* in Fig. 6, Δh_* is approximately 10% for the entire channel at any time, regardless of the developmental state of the alternate bars. In all the areas where Δh_* is 60% or more, the water depth is very shallow. Most of these regions are not included when calculating the migrating speed. This is demonstrated from the plan view of the migrating speed in Fig. 10 that is shown in the next section. Therefore, we decided to use the calculated value of this part as well. In the next section, we verify the applicability of the derived calculation formulas using these hydraulic quantities.

4.2 Verifying the Application of the Time Waveform for the Bed Level and the Riverbed Fluctuation Amount

We verified the applicability of the calculation formula that is derived in the previous section from two points of view. First, can the time waveform of the measured bed level be reproduced? Second, can the riverbed fluctuation amount that is measured in the entire section be reproduced? The verification results are described in this section.

4.2.1 Bed-level Time Waveform

The verification method that uses the time waveform at the bed level is described here. The HPDE from Eq. (14) that was derived in the previous section is numerically calculated as follows, and the amount of the riverbed fluctuation is between Δt.

$$\Delta z = \left(-M_x \frac{\partial z}{\partial x} - M_x I_{ex} - M_x F_x - M_y \frac{\partial z}{\partial y} - M_y I_{ey} - M_y F_y \right) \Delta t \tag{19}$$

This calculation used the bed level and water depth that is measured with ST, as well as the calculated values of the energy slope and flow velocity based on the hydraulic analysis that was described in the previous section. A time waveform at the bed level was obtained by repeating this numerical integration during each ST measurement time.

The applicability of the HPDE that was obtained in the previous section was investigated by comparing the time waveform of the bed level. This was calculated using the aforementioned method with the time waveform of the bed level that was observed by the ST. In this study, because the ST measurements were performed at 1-min intervals, Δt in the aforementioned calculation was set to 1 min.

Figure 8 shows the time waveform at the bed level. Figure 8 shows the time waveforms of (a) the left bank side, (b) central part, and (c) right bank side at 6.0 m from the upstream end; the red line shows the bed level of the measured value. In the figure, the blue line shows the bed level that is calculated from the calculation formula. By focusing on the measured values that are shown by the red line in Fig. 8, (a) the bed level decreases on the left bank side, and (b) the bed level increases on the central part and (c) right bank side from the start of the water flow to 50 min. In addition, it can be observed that the bed level of (a) and (b) settled down

and the bed level of (c) increased from 50 to 150 min for the water flow. After 150 min, the bed level increased slightly for (a), (b), and (c).

Next, by looking at the time waveform of the bed level with the calculation formula, the time waveform of the bed level is well reproduced from the start of the water flow to 100–120 min in Figures (a), (b), and (c). It can be confirmed that after 100 min, the reproducibility decreases on (a) the left bank side; after 150 min, the reproducibility decreases on (b) the center and (c) the right bank side. By overlooking the process from the occurrence to the development of alternate bars using Fig. 4 and Fig. 8, it was confirmed that the reproducibility of the time waveform, when the propagation of the alternate bars is remarkable, is good. Conversely, it was determined that the reproducibility becomes poor, especially in the sedimentary part when the propagation of the alternate bars is slow.

As mentioned earlier, the time waveform was obtained by setting the time integration interval to 1 min. Although this time interval cannot be simply compared, it is much larger than the time interval in a general numerical analysis. From this result, it was determined that the verification method that uses the aforementioned numerical integration and the applicability of the calculation formula that was derived in the previous section are excellent.

4.2.2 Riverbed Variation Amount

The verification in the previous section showed that the HPDE for Eq. (14) has sufficient applicability, but its applicability decreases as the alternate bars develop. In this section, we discuss how much of this reduced applicability occupies the entire waterway and where it occurs. This is achieved using the riverbed variation amount. The verification of the riverbed variation was performed using the following equation.

$$\Delta z_* = |\Delta z_{obs} - \Delta z_{cal}|/d \times 100 \tag{20}$$

where Δz_{obs} is the riverbed variation that was obtained from the bed level between the two times that were measured by the ST. In addition, Δz_{cal} is the amount of the riverbed variation by the HPDE and the calculation formula of the migration speed. Δz_* in the aforementioned equation is a dimensionless quantity that is obtained by dividing the difference between the measured value of the riverbed variation amount and the calculated value using the equation based on the particle size. In addition, the difference between the two shows how much the divergence is based on the particle size.

Figure 9 shows the plan view for the calculation accuracy of the riverbed variation Δz_*. Figure 9 shows the bed level, Δz_* from the top. In addition, (a) to (i) indicates the time zone in which the change is remarkable from the occurrence to the development at 10-min intervals. In addition, (i) to (l) indicates the time zone in which the change is slow until the end of the water flow at 40-min intervals. (a) Looking at the results for 1 min of water flow, Δz_* is generally within 100%, and the estimation accuracy of the waveform after 1 min at this time is the same as the particle size.

From (a) 1 min of water flow to (h) 70 min, it can be observed that Δz_* is generally within 100% of the entire channel. However, it can be observed that Δz_* increases at the front edge of the bar after 80 min of water flow in comparison to the other areas. From this, it is inferred that the applicability of this formula decreases at the front edge of the alternate bars where the water depth becomes shallow. Presently, the factors that reduce the applicability of the calculation formula have not been sufficiently identified; however, it is suggested that careful handling is required in places where the water depth becomes shallow. Conversely, it is unlikely

that alternate bars with a high wave height such that the water depth becomes extremely shallow as considered in this experiment actually exists in an actual river; therefore, it is considered that the decrease in applicability at the aforementioned points is acceptable. It should be noted that there is a striped area where Δz_* is close to 500% on the side wall of the figure. This area is considered to occur owing to a decrease in the ST measurement accuracy. In addition, (b) an increase in Δz_* at the upstream end for 10 min of water flow is considered to occur owing to the same aforementioned reason. Therefore, in the following discussion, the striped pattern of Δz_* on the right bank side and Δz_* at the upstream end were excluded from consideration.

5 Quantification of the Migrating Speed for the Alternate Bars

The previous section confirmed that HPDE and the calculation formula for the migrating speed can reproduce the propagation phenomenon of the alternate bars. In this section, the migration speed of the alternate bars in each process during the occurrence and development is quantified using the calculation formula of the migrating speed.

5.1 Spatial Distribution of the Migrating Speed of the Alternate Bars

Figure 10 shows a plan view of the dimensionless migrating speed that is obtained by dividing the migrating speed that is obtained from the calculation formula for the bed level by the initial uniform flow velocity. The dimensionless migrating speed was used to understand the magnitude of the running water velocity and bed velocity. In a stability analysis(Callander, 1969; Kuroki & Kishi, 1984) that was conducted in the past, by applying the dimensionless governing equation, the migrating speed that was made dimensionless during the uniform velocity flow is often used.

The figure shows the bed level and M/u_0 from the top. M is the magnitude migrating speed, u_0 is the uniform flow velocity. The area surrounded by the hatch in the figure is the area in which the Shields number does not exceed the critical Shields number (hereinafter referred to as the effective Shields number); in this area, the migrating speed is 0. It is demonstrated that (a) to (i) indicates the time zone in which the change is significant from the occurrence to the development of the alternate bars at 10-min intervals. In addition, (i) to (l) indicates the time zone in which the change is slow until the end of the water flow at 40-min intervals. It should be noted that the colors of the case law regarding the bed level and M/u_0 are different between (a) to (h) and (i) to (l).

First, by focusing on (a) 1 min of water flow in the figure, M/u_0 has almost no spatial distribution on a floor with an almost flat bed. It is also confirmed that the bed surface propagates uniformly at a speed of approximately 0.002. After the bed changes slightly from (b) 10 min to (c) 20 min, M/u_0 begins to have a spatial distribution. Subsequently, the spatial distribution of M/u_0 changes significantly from (d) 30 min of water flow to (e) 40 min when the alternate bars occurred. Looking at this change with a spatial distribution from place to place, it can be observed that M/u_0 increases at the sedimentary part and the front edge of the alternate bars, and it decreases at other places. Subsequently, the spatial distribution of M/u_0 became clearer from (f) 50 min to (i) 80 min. In addition, before this time, it can be demonstrated that the area, where migrating speed is zero, is expanded on the downstream side of the front edge. In addition, (i) M/u_0 at 80 min of water flow decreased to approximately 0.001 or less, while excluding the sedimentary part. (l) The spatial distribution of the migrating speed at 240 min of the final time is not significantly different from the distribution of (i) 80 min, but the area, where migrating speed

is zero, is further expanded. In addition, M/u_0 also decreases slightly in the entire channel.

Next, Fig. 11 illustrates a histogram that quantitatively shows the spatial distribution degree of M/u_0 at each time. The red and blue vertical lines in the figure represent the mean and mean ± standard deviation of M/u_0 at each time, and each value is shown at the top of the figure. First, (a) the shape of the histogram after 1 min of water flow was concentrated around the average value of 0.157. In addition, because the standard deviation is 0.029, which is small with respect to the mean value, it can be observed that the spatial distribution of M/u_0 at this time is small. Then, from (b) 10 min of water flow to (e) 40 min of water flow when the alternate bars occurred, the shape of the histogram became flat, and the mean value of M/u_0 was 0.147, and the standard deviation was 0.051. Comparing (a) 1 min and (e) 40 min of water flow, although the mean value decreased by approximately 4 %, the standard deviation increased to nearly 40 % of the mean value. From this, it is demonstrated that the spatial distribution of the migrating speed greatly expanded from the flat bed to the occurrence of the alternate bars. After that, from (e) 40 min to (i) 80 min of water flow, the flattening of the histogram, the increase in the standard deviation, and the decrease in the mean value of M/u_0 became more significant. From this, the increase in the standard deviation is particularly significant, and the standard deviation value during 80 min of water flow reaches 70 % of the average value of M/u_0. (i) After 80 min of water flow, there is no significant change from (e) to (i). However, the average value of M/u_0 gradually increases over 240 min of the final time, and it decreases and the standard deviation increases. Comparing (a) 1 min of water flow and (k) 240 min, which was the final time, the mean value of M/u_0 is 0.72 times, and the standard deviation is 4.8 times.

From these results, it was demonstrated that the migration speed of the alternate bars has a spatial distribution, and this spatial distribution expands from the stage of occurrence to the development of the alternate bars.

5.2 Scale of the Migrating Speed of the Alternate Bars

This section discusses the scale of the migration speed of the alternate bars. As shown in the previous section, from Fig. 11, it can be confirmed that the migrating speed has a spatial distribution and it gradually expands from 1 min of water flow to 240 min, which was the final time. The non-dimensional migrating speed in the figure is divided by the uniform flow velocity (0.28 m/s) on the flat floor. However, the scale of the migrating speed is on the order of 10^{-4} to 10^{-3} of the uniform flow velocity at any place, regardless of the developmental state of the alternate bars. Therefore, it is inferred that the deformation rate of the bed surface is sufficiently smaller than the deformation rate of the running water. This tendency is similar to the result of the non-dimensional migrating speed that corresponds to the wave number of the maximum development rate as described by Callander(Callander, 1969).

6 Discussion

In the previous sections, it was clarified that the migration speed of the alternate bars has a spatial distribution, and this spatial distribution changes with time. This section discusses the following three aspects of the migration speed of the alternate bars.

6.1 Approximate Description of the most Dominant Physical Quantity of the Migrating Speed

This study derived a formula to calculate the migration speed and its applicability is confirmed. Therefore, by considering the mathematical structure of the same formula, it is possible to determine the most dominant physical quantity that controls the migration speed. As demonstrated in Eq. (15) and Eq. (16), the dominant physical quantities of the migrating speed are the Shields number and energy slope, which excludes the component decomposition of the migrating speed. Because the dominant physical quantities of the Shields number consist of the water depth and energy slope, it can be concluded that the dominant physical quantities of the migrating speed are the water depth and energy slope. In addition, the migrating speed is calculated by multiplying the depth and the energy slope as shown in Eq. (15) and Eq. (16). The depth in a river with alternate bars is generally on the order of 10^0, and the energy slope in the rivers with alternate bars is on the order of 10^{-2} to 10^{-4}. Therefore, because the migration speed is the product of the water depth and energy slope, it is inferred that the energy slope is dominant in terms of regulating the magnitude of the migrating speed.

Figure 12 shows the relationship between the depth, energy slope, and migrating speed at each time. As demonstrated in Fig. 12, the relationship between the energy slope and migrating speed is nearly linear. Regarding the relationship between the depth and migrating speed, the migrating speed decreased with an increasing depth. From these results, it can be demonstrated that the migrating speed of the alternate bars is defined according to the energy slope.

It was previously demonstrated that the dominant physical quantity of the migrating speed is the energy slope. It is believed that an approximate description of the migrating speed is possible using the energy slope and a water surface slope, which is very similar to the energy slope. We verified whether the above approximate description is possible from Fig. 13. The red points show the relationship between M/u_0 and $0.4 \times I_e$, and the green point shows M/u_0 and $0.4 \times I_w$ in Fig. 13. I_w is the value that is obtained by the central spatial difference of the water level that is measured by the ST. Each correlation coefficient is shown on the upper side of Fig. 13. Furthermore, 0.4, which is multiplied by I_e and I_w, is a coefficient that is determined by the particle size. This is one of the variables on the denominator side of Eq. (15) and Eq. (16).

First, it can be observed that the relationship between M/u_0 and $0.4 \times I_e$ is a nearly one-to-one relationship at all times. Furthermore, both relationships have a highly positive correlation because the correlation coefficients are over 0.99, on average. Second, it can be demonstrated that there is some variation in the relationship between M/u_0 and $0.4 \times I_w$, but it is also a nearly one-one relationship at all times. Furthermore, both relationships have a highly positive correlation because the correlation coefficients are over 0.96 on average.

From these results, it was determined that the dominant physical quantity of the alternate bars is the energy slope, and the migration speed can be approximated using the energy slope and water surface slope.

6.2 Comparison of the Migrating Speed and the Stability Analysis

The migration speed based on the stability analysis(Callander, 1969; Kuroki & Kishi, 1984) has four dominant physical quantities: the Froude number, Shields number, bed slope, and wavenumber. In addition, the migration speed that was obtained from the HPDE, which was discussed in the previous section, is dominated by the Shields number and energy slope. The migration speed that was obtained from

each stability analysis and the HPDE both have the water depth and energy slope as the dominant physical quantities. However, the migration speed that was obtained from the stability analysis was limited to those that correspond to any wavenumber.

6.3 Decreasing Factor for the Migrating Speed of the Alternate Bars

This subsection discusses the decreasing factor for the migrating speed of the alternate bars. Figure 14 shows the average longitudinal distributions of the migrating speed, energy line, hydraulic grade line, and bed line over time. The sediment condition for the flume experiment in this study is that there is no sediment supply. Therefore, this study confirmed that the bed level decreases with the passage of time along the upstream side of the movable bed. At the final time, the bed level decreased significantly from the upstream end to a point that is 3.5 m away. It can be demonstrated that (b) the water level and energy head in this section have decreased compared to the initial stage, and the riverbed slope and energy slope become more gentle. In addition, (a) the migrating speed, which was calculated from Eq. (15) at the final time in this section, is lower than that during the beginning of the water flow.

A previous study by Eekhout et al. (Eekhout et al., 2013), which observed the occurrence and development process of the alternate bars in rivers, reported that the bed slope decreased while reducing the migration speed of the alternate bars. The results shown in Fig. 14 are consistent with those reported by Eekhout et al.

As mentioned earlier, the dominant physical quantity of the migrating speed of the alternate bars is the energy slope. The decrease in the migrating speed, which was confirmed by the flume experiments in this study and the observations in the actual river by Eekhout et al., should be interpreted as a decrease in the migration speed of the alternate bars due to the decrease in the riverbed slope rather than the decrease in the migrating speed with the development of the alternate bars.

7 Conclusion

In this study, we first conducted a flume experiment under the condition that alternate bars can occur and develop. We measured the hydraulic quantity and bed shape with a high spatial resolution. Next, we quantified the migrating speed of the alternate bars using the measured values that were obtained in the flume experiment and the calculation formula. This study determined that the migration speed of the alternate bars has a spatial distribution and it changes with time. The results of this study are presented below.

1) We were able to measure the water level and bed level with a high resolution while continuing the water flow. In addition, the water level and bed level of the occurrence and development process of the alternate bars are measured, and it is demonstrated that the migrating speed of the alternate bars has a spatial distribution from the measured geometric shape of the bed surface.
2) The HPDE for the bed level z and the formula of the migrating speed were derived to quantitatively determine the migrating speed of the alternate bars. By comparing the measured values of the flume experiment, it was demonstrated that the formula can appropriately describe the propagation phenomenon of the alternate bars.
3) By calculating the migrating speed of the alternate bars based on the aforementioned formula, it was clarified that the migrating speed of the alternate bars has a spatial distribution. In addition, the spatial distribution changes with the development of the bars over time, which was unconfirmed in the literature.

4) The dominant physical quantity of the migrating speed is the energy slope based on the results of the experiment and calculation formula. In addition, by comparing the scales of I_e and I_w with the non-dimensional migrating speed, it is suggested that the non-dimensional migrating speed can be described using I_e and I_w; the behavior of the bars in the rivers can also be explained by I_e and I_w.
5) It was observed that the migrating speed of the alternate bars is about three to four orders of magnitude smaller than the initial uniform flow velocity, regardless of the developmental state and the location of the bars.

It was found that the decrease in the applicability of the HPDE for the bed level and calculation formula of migration speed for the alternate bars, which was derived in this study, occurs in the sediment parts with extremely shallow water depth. Therefore, it is difficult to apply the aforementioned formula. However, it is unlikely that alternate bars, which has sediment parts with extremely shallow water depth, will occur in actual rivers, so this problem is not considered to be a practical problem.

Previous studies have revealed that the bank failure and the channel evolution are closely related to alternate bars (Ryosaku, 1957; Callander, 1969). In the future, we will quantify the spatial distribution of the migration speed of alternate bars in actual rivers, and consider the above relationship.

Acknowledgments

The data used in this study can be accessed at https://doi.org/10.4121/14384999. For details of the data, please refer to the enclosed README.md. We would like to thank Editage (www.editage.com) for English language editing.

References

Callander, R. A. (1969). Instability and river channels. *Journal of Fluid Mechanics*, *36*(3), 465-480. doi: 10.1017/S0022112069001765

Colombini, M., Seminara, G., & Tubino, M. (1987). Finite-amplitude alternate bars. *Journal of Fluid Mechanics*, *181*, 213-232. doi: 10.1017/S0022112087002064

Colombini, M., & Tubino, M. (1991). Finite-amplitude free bars: A fully nonlinear spectral solution. *in Sand Transport in Rivers, Estuaries and the Sea, edited by R. Soulsby and R. Bettes*, *A. A. Balkema, Brookfield, Vt.*, 163-169.

Crosato, A., Desta, F. B., Cornelisse, J., Schuurman, F., & Uijttewaal, W. S. J. (2012). Experimental and numerical findings on the long-term evolution of migrating alternate bars in alluvial channels. *Water Resources Research*, *48*(6). doi: 10.1029/2011WR011320

Crosato, A., Mosselman, E., Beidmariam Desta, F., & Uijttewaal, W. S. J. (2011). Experimental and numerical evidence for intrinsic nonmigrating bars in alluvial channels. *Water Resources Research*, *47*(3). doi: 10.1029/2010WR009714

Doelman, A., de Swart, H., & Schielen, R. (1993, 07). On the non-linear dynamics of free bars in straight channel. *Journal of Fluid Mechanics*, *252*, 325 - 356. doi: 10.1017/S0022112093003787

Eekhout, J. P. C., Hoitink, A. J. F., & Mosselman, E. (2013). Field experiment on alternate bar development in a straight sand-bed stream. *Water Resources Research*, *49*(12), 8357-8369. doi: 10.1002/2013WR014259

Federici, B., & Seminara, G. (2003). On the convective nature of bar instability. *Journal of Fluid Mechanics*, *487*, 125-145. doi: 10.1017/S0022112003004737

Fujita, Y., Koike, T., Furukawa, R., & Y., M. (1985). Experiments on the initial stage of alternate bar formation. *Disaster Prevention Research Institute Annuals (in Japanese)*, *28*(B-2), 379-398.

Fujita, Y., & Muramoto, Y. (1985). Studies on the process of development of alternate bars. *Bulletin of the Disaster Prevention Research Institute*, *30(3)*, 55-86.

Ikeda, H. (1983). Experiments on bedload transport, bed forms, and sedimentary structures using fine gravel in the 4-meter-wide flume..

Kennedy, J. F. (1963). The mechanics of dunes and antidunes in erodible-bed channels. *Journal of Fluid Mechanics*, *16*(4), 521-544. doi: 10.1017/S0022112063000975

Kuroki, M., & Kishi, T. (1984). Regime criteria on bars and braids in alluvial straight channels. *Proceedings of the Japan Society of Civil Engineers*, *1984*(342), 87-96. doi: 10.2208/jscej1969.1984.342_87

Lanzoni, S. (2000a). Experiments on bar formation in a straight flume: 1. uniform sediment. *Water Resources Research*, *36*(11), 3337-3349. doi: 10.1029/2000WR900160

Lanzoni, S. (2000b). Experiments on bar formation in a straight flume: 2. graded sediment. *Water Resources Research*, *36*(11), 3351-3363. doi: 10.1029/2000WR900161

Miwa, H., Daisdo, A., & Katayama, T. (2007). Effects of water and sediment discharge conditions on variation in alternate bar morphology. *Proceedings of hydraulic engineering (in japanese)*, *51*, 1051-1056. doi: 10.2208/prohe.51.1051

Nobuhisa, N., Yoshio, M., Yoshihiko, U., Takashi, H., Masayuki, Y., Yasuhiko, T., & Michiaki, I. (1999). On the behaviour of alternate bars under several kinds of channel conditions. *PROCEEDINGS OF HYDRAULIC ENGINEERING (in japanese)*, *43*, 743-748. doi: https://doi.org/10.2208/prohe.43.743

Podolak, C. J. P., & Wilcock, P. R. (2013). Experimental study of the response of a gravel streambed to increased sediment supply. *Earth Surface Processes and Landforms*, *38*(14), 1748-1764. doi: 10.1002/esp.3468

Ryosaku, K. (1957). Formation of "dunes" on river-bed. *Transactions of the Japan Society of Civil Engineers in Japan(in Japanese)*, *1957*(42), 1-21. doi: 10.2208/jscej1949.1957.1

Ryosaku, K. (1958). Experiment on dune length in straight channel. *Journal of the Japan Society of Erosion Control Engineering (in japanese)*, *1958*(30), 1-8. doi: 10.11475/sabo1948.1958.30_1

Ryosaku, K. (1961). Investigation of channel deformation in ishikari river. *Rep. Bureau of Resources, Dept. Science & Technology, Japan. (in japanese)*.

Seminara, G. (2010). Fluvial sedimentary patterns. *Annual Review of Fluid Mechanics*, *42*(1), 43-66. doi: 10.1146/annurev-fluid-121108-145612

Shimizu, Y., & Itakura, T. (1989). Calculation of bed variation in alluvial channels. *Journal of Hydraulic Engineering*, *115*(3), 367-384. doi: 10.1061/(ASCE)0733-9429(1989)115:3(367)

Tubino, M. (1991). Growth of alternate bars in unsteady flow. *Water Resources Research*, *27*(1), 37-52. doi: 10.1029/90WR01699

Venditti, J. G., Nelson, P. A., Minear, J. T., Wooster, J., & Dietrich, W. E. (2012). Alternate bar response to sediment supply termination. *Journal of Geophysical Research: Earth Surface*, *117*(F2). doi: 10.1029/2011JF002254

Yuichi, I. (1956). Hydrodynamical study on critical tractive force. *Transactions of the Japan Society of Civil Engineers (in Japanese)*, *1956*(41), 1-21. doi: 10.2208/jscej1949.1956.41_1

Zhang, Z. (2000). A flexible new technique for camera calibration. *IEEE Transactions on Pattern Analysis and Machine Intelligence*, *22*(11), 1330-1334. doi: 10.1109/34.888718

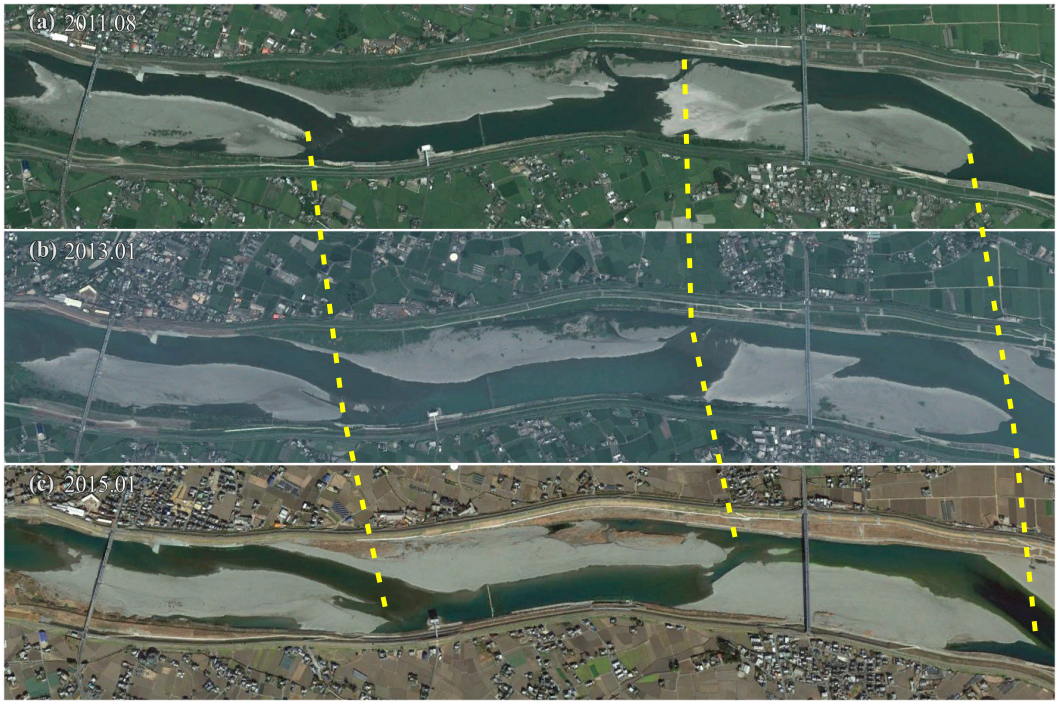

Figure 1. Aerial photos in the Naka river of Japan. © Google Earth

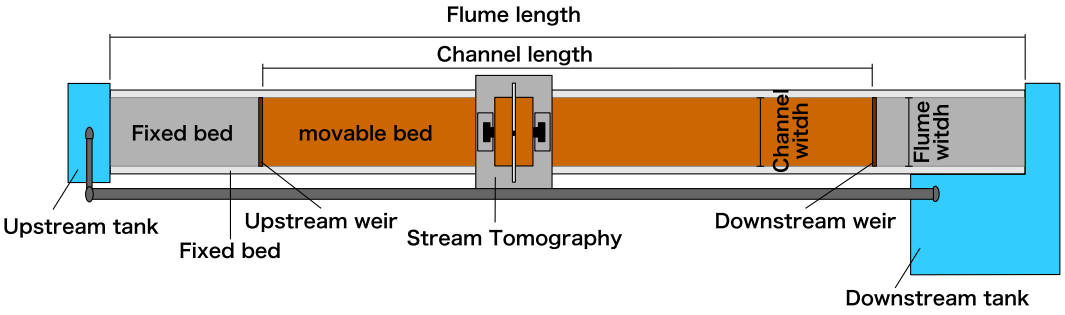

Figure 2. Plan view of the experiment flume

Appendix A Stream Tomography

Here, we describe the measurement principle of the stream tomography that was used in the flume experiment.

A1 Outline of the Measurement Device and Measurement Procedure

Figure A1 and Fig. A2 show the overall plan view of the measurement device and the layout of the equipment. The overall configuration of the measurement device consists of a laser sheet light source and a traveling platform that has two digital cameras installed. The laser sheet light source that was used in this study is a yttrium aluminum garnet (YAG) laser with a wavelength of 532 nm. In addition, in order to promote the emission of the laser light in water, the water that was used in the flume experiment was green from dissolving sodium fluorescein. As shown in Fig. A1 and Fig. A2, the two digital cameras sandwich the laser sheet light source so it

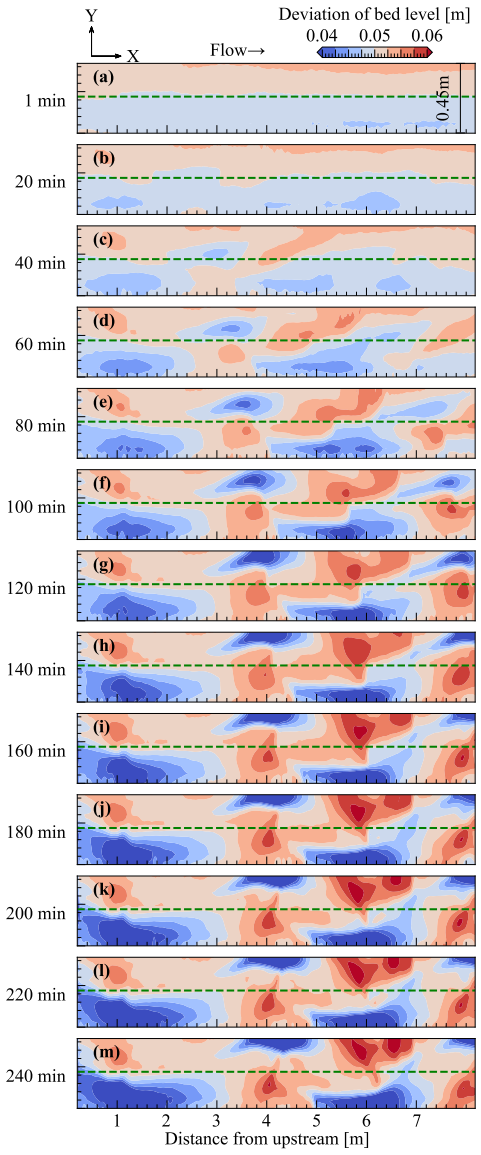

Figure 3. Temporal changes of the plan view in the observed bed topography

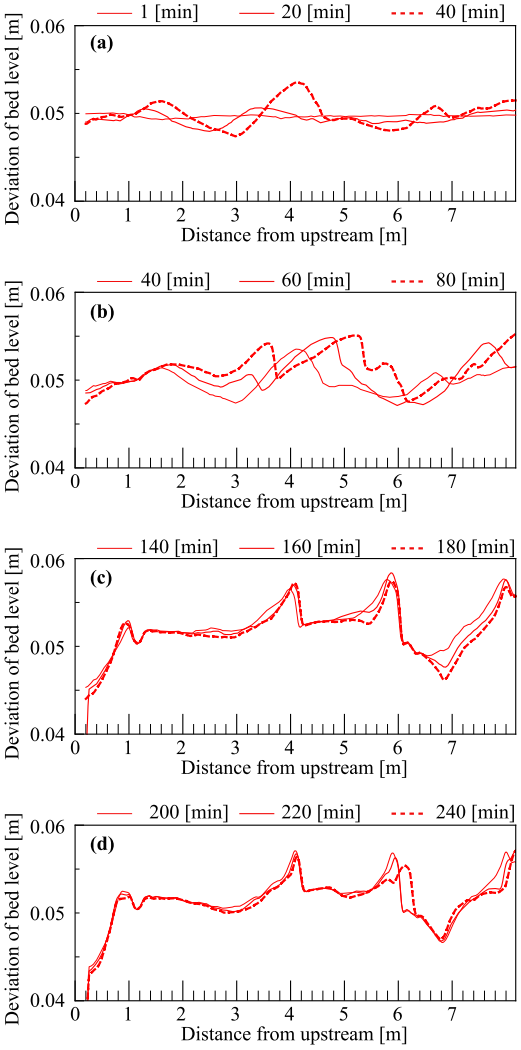

Figure 4. Longitudinal view of the measured bed shape. (a) Initial stage of the experiment, (b) occurrence of the alternate bars, (c) intermediate stage of the experiment, and (d) the final stage of the experiment

was upstream and downstream on the traveling platform. The camera was installed so that it looks diagonally downward toward the center of the stream. The three-dimensional coordinates of the water level and bed level by the ST can be obtained based on the intersection of the origin coordinates (lens center point) for each of the two aforementioned cameras and the geometric vector that connects the water level and bed position that will be measured.

ST is a non-contact measurement method that is based on triangulation and it is used for photogrammetry. The geometric relationship in this method is shown in the figures. The water level is obtained as the intersection of the two geometric vectors that connect the origin coordinates for each of the two cameras and the water surface. The bed level can be determined as the intersection of the two geometric vectors for the aforementioned water level and bed level. From these, the calculation

of the three-dimensional coordinates of the bed level requires consideration of the refraction of the irradiation light on the water surface. The three-dimensional coordinates of the bed level can be obtained using a geometric vector that considers the refraction of the irradiation light. This refraction is based on the surface water level that was obtained by this method.

The measurement procedures consist of the following three stages. 1) Movie shooting: a camera was installed on the traveling platform while running it in the longitudinal direction. 2) Image analysis: after decomposing the shot video into still photos, the pixel number that corresponds to the intersection of the bed and water with laser light is calculated. 3) The water level and bed level are obtained by triangulation. The following sections show the geometric calculations based on the image analysis and triangulation. In addition, it can be obtained either before or after the movie shooting that was described in 1). Zhang's calibration method (Zhang, 2000) was used to calculate the internal and external parameters of the camera. The origin coordinates of the cameras that were installed on the upstream and downstream sides of the waterway are $\boldsymbol{c_u}$ and $\boldsymbol{c_d}$, respectively. $\boldsymbol{c_u}$ and $\boldsymbol{c_d}$ are the number vectors whose components are three-dimensional spatial coordinates, and $\boldsymbol{c_u} = (x_{c_u}, y_{c_u}, z_{c_u})$ and $\boldsymbol{c_d} = (x_{c_d}, y_{c_d}, z_{c_d})$.

A2 Geometric Calculation of the Water Level and Bed Level based on the Image Analysis and Triangulation

The method for detecting the water surface and bed surface in the ST is described as follows. From the still photograph that was created from the moving image captured by the camera, the pixel number corresponding to the intersection of the laser beam and the water surface, and the intersection of the laser beam and the water bed was calculated. First, the pixel number (i_w, j_w) corresponding to the intersection of the laser beam and the water surface is detected using the green brightness of the photograph as the threshold value. Similarly, the pixel numbers (i_b, j_b) corresponding to the intersection of the laser beam and the bed surface are distinguished from the position of the maximum green brightness. The reflection intensity on the water surface and bed surface varies depending on the environment, laser light intensity, and the riverbed material. Therefore, it is necessary to adjust the thresholds for detecting the water and bed surfaces according to the measurement conditions. The threshold value for the green lightness in this analysis was set to 40–210.

Next, the geometric calculation of the water level is explained. The water level was calculated from the geometric relationship that is shown in Fig. A4. The three-dimensional coordinates of the water level $\boldsymbol{h}$ are obtained as the intersection of $\boldsymbol{c_{wu}}$ and $\boldsymbol{c_{wd}}$. $\boldsymbol{c_{wu}}$ is a geometric vector connecting $\boldsymbol{c_u}$ and the water surface level to be measured $\boldsymbol{c_u}$. $\boldsymbol{c_{wd}}$ is a geometric vector connecting $\boldsymbol{c_d}$ and the water surface level to be measured $\boldsymbol{c_d}$. In this method, the nearest points $\boldsymbol{h_u}$ and $\boldsymbol{h_d}$ for these geometric vectors were calculated. The threshold values are set, which can be regarded as the closest distance between the two points; the intersections are identified $\boldsymbol{h}$ when it is below the threshold value. The latest points are calculated using the following equations.

$$\boldsymbol{h_u} = \boldsymbol{c_u} + \boldsymbol{d_{cu}}\hat{\boldsymbol{c}}_{\boldsymbol{wu}} \tag{A1}$$

$$\boldsymbol{h_d} = \boldsymbol{c_d} + \boldsymbol{d_{cd}}\hat{\boldsymbol{c}}_{\boldsymbol{wd}} \tag{A2}$$

$$\boldsymbol{d_{cu}} = \frac{(\hat{\boldsymbol{c}}_{\boldsymbol{wd}} \cdot \hat{\boldsymbol{c}}_{\boldsymbol{wu}})(\hat{\boldsymbol{c}}_{\boldsymbol{wd}} \cdot c_d\vec{c}_u) - \hat{\boldsymbol{c}}_{\boldsymbol{wu}} \cdot c_d\vec{c}_u}{1 - (\hat{\boldsymbol{c}}_{\boldsymbol{wd}} \cdot \hat{\boldsymbol{c}}_{\boldsymbol{wu}})(\hat{\boldsymbol{c}}_{\boldsymbol{wd}} \cdot \hat{\boldsymbol{c}}_{\boldsymbol{wu}})} \tag{A3}$$

$$\boldsymbol{d_{cu}} = \frac{(\hat{\boldsymbol{c}}_{\boldsymbol{wu}} \cdot \hat{\boldsymbol{c}}_{\boldsymbol{wd}})(\hat{\boldsymbol{c}}_{\boldsymbol{wu}} \cdot c_u\vec{c}_d) - \hat{\boldsymbol{c}}_{\boldsymbol{wd}} \cdot c_u\vec{c}_d}{1 - (\hat{\boldsymbol{c}}_{\boldsymbol{wu}} \cdot \hat{\boldsymbol{c}}_{\boldsymbol{wd}})(\hat{\boldsymbol{c}}_{\boldsymbol{wu}} \cdot \hat{\boldsymbol{c}}_{\boldsymbol{wd}})} \tag{A4}$$

$$\boldsymbol{h} = \frac{1}{2}(\boldsymbol{h_u} + \boldsymbol{h_d}) \tag{A5}$$

where $\boldsymbol{h}$ is a number vector whose components are the three-dimensional coordinates of the calculated water level, and $\boldsymbol{h_u}$ and $\boldsymbol{h_d}$ are the number vectors of the bed level. These are calculated based on the origin coordinates of the upstream and downstream cameras. In addition, $\boldsymbol{c_{\hat{wu}}}$ and $\boldsymbol{c_{\hat{wd}}}$ are the unit vectors of $\boldsymbol{c_{wu}}$ and $\boldsymbol{c_{wd}}$.

The water level in the transverse direction is calculated using the aforementioned calculation. This calculation is repeated for the image that is taken by the traveling platform that is moving at a constant speed. As a result, transverse water surface shapes in multiple longitudinal directions were obtained, and the surface shape of the water level was obtained by combining these. During the final processing, $H_{(i,j)}$ is obtained. This is a structural discrete function that is rearranged in a grid pattern at arbitrary intervals that is based on $\boldsymbol{h}$.

Next, the geometric calculation of the bed level is explained. The bed level was calculated from the geometric relationship as shown in Fig. A5. As illustrated in the figure, $\boldsymbol{c_{biu}}$ and $\boldsymbol{c_{bid}}$, which are the geometric vectors that are incident in water, are refracted on the water surface. The intersections of the geometric vector after refracting from $\boldsymbol{c_{bru}}$ and $\boldsymbol{c_{brd}}$ are the bed pixels (i_b, j_b) on the image.

Therefore, to calculate the bed level, it is necessary to obtain the geometric vectors $\boldsymbol{c_{bru}}$ and $\boldsymbol{c_{brd}}$. Here, to prepare for the aforementioned calculation, the intersections $\boldsymbol{c_{hu}}$ and $\boldsymbol{c_{hd}}$ for the water surface and both of the geometric vectors $\boldsymbol{c_{biu}}$ and $\boldsymbol{c_{bid}}$ can be calculated. $\boldsymbol{c_{bru}}$ and $\boldsymbol{c_{brd}}$ can be calculated from the following equations while using $H_{(i,j)}$, which is arranged in a grid, and $\boldsymbol{c_{biu}}$ and $\boldsymbol{c_{bid}}$.

$$\boldsymbol{\acute{c}_{hu}} = \boldsymbol{c_u} + \boldsymbol{c_{biu}} \frac{\overrightarrow{H_{(i,j)}\boldsymbol{c_u}} \cdot \boldsymbol{n_u}}{\overrightarrow{H_{(i,j)}\boldsymbol{c_u}} \cdot \boldsymbol{n_u} + \overrightarrow{H_{(i,j)}\boldsymbol{c_{eu}}} \cdot \boldsymbol{n_u}} \tag{A6}$$

$$\boldsymbol{a_{u1}} = \overrightarrow{H_{(i,j)}H_{(i+1,j)}} \times \overrightarrow{H_{(i+1,j)}\boldsymbol{\acute{c}_{hu}}} \tag{A7}$$

$$\boldsymbol{a_{u2}} = \overrightarrow{H_{(i+1,j)}H_{(i,j+1)}} \times \overrightarrow{H_{(i,j+1)}\boldsymbol{\acute{c}_{hu}}} \tag{A8}$$

$$\boldsymbol{a_{u3}} = \overrightarrow{H_{(i,j+1)}H_{(i,j)}} \times \overrightarrow{H_{(i,j)}\boldsymbol{\acute{c}_{hu}}} \tag{A9}$$

$$\boldsymbol{b_{u1}} = \overrightarrow{H_{(i+1,j+1)}H_{(i,j+1)}} \times \overrightarrow{H_{(i,j+1)}\boldsymbol{\acute{c}_{hu}}} \tag{A10}$$

$$\boldsymbol{b_{u2}} = \overrightarrow{H_{(i,j+1)}H_{(i+1,j)}} \times \overrightarrow{H_{(i+1,j)}\boldsymbol{\acute{c}_{hu}}} \tag{A11}$$

$$\boldsymbol{b_{u3}} = \overrightarrow{H_{(i+1,j)}H_{(i+1,j+1)}} \times \overrightarrow{H_{(i+1,j+1)}\boldsymbol{\acute{c}_{hu}}} \tag{A12}$$

if ($\boldsymbol{a_{\hat{u}1}}$=$\boldsymbol{a_{\hat{u}2}}$=$\boldsymbol{a_{\hat{u}3}}$) or ($\boldsymbol{b_{\hat{u}1}}$=$\boldsymbol{b_{\hat{u}2}}$=$\boldsymbol{b_{\hat{u}3}}$) then,

$$\boldsymbol{c_{hu}} = \boldsymbol{\acute{c}_{hu}} \tag{A13}$$

$$\boldsymbol{\acute{c}_{hd}} = \boldsymbol{c_d} + \boldsymbol{c_{bid}} \frac{\overrightarrow{H_{(i,j)}\boldsymbol{c_d}} \cdot \boldsymbol{n_d}}{\overrightarrow{H_{(i,j)}\boldsymbol{c_d}} \cdot \boldsymbol{n_d} + \overrightarrow{H_{(i,j)}\boldsymbol{c_{ed}}} \cdot \boldsymbol{n_d}} \tag{A14}$$

$$\boldsymbol{a_{d1}} = \overrightarrow{H_{(i,j)}H_{(i+1,j)}} \times \overrightarrow{H_{(i+1,j)}\boldsymbol{\acute{c}_{hd}}} \tag{A15}$$

$$\boldsymbol{a_{d2}} = \overrightarrow{H_{(i+1,j)}H_{(i,j+1)}} \times \overrightarrow{H_{(i,j+1)}\boldsymbol{\acute{c}_{hd}}} \tag{A16}$$

$$\boldsymbol{a_{d3}} = \overrightarrow{H_{(i,j+1)}H_{(i,j)}} \times \overrightarrow{H_{(i,j)}\boldsymbol{\acute{c}_{hd}}} \tag{A17}$$

$$\boldsymbol{b_{d1}} = \overrightarrow{H_{(i+1,j+1)}H_{(i,j+1)}} \times \overrightarrow{H_{(i,j+1)}\boldsymbol{\acute{c}_{hd}}} \tag{A18}$$

$$\boldsymbol{b_{d2}} = \overrightarrow{H_{(i,j+1)}H_{(i+1,j)}} \times \overrightarrow{H_{(i+1,j)}\boldsymbol{\acute{c}_{hd}}} \tag{A19}$$

$$\boldsymbol{b_{d3}} = \overrightarrow{H_{(i+1,j)}H_{(i+1,j+1)}} \times \overrightarrow{H_{(i+1,j)}\acute{\boldsymbol{c}}_{\boldsymbol{hd}}} \tag{A20}$$

if ($\hat{\boldsymbol{a}}_{\boldsymbol{d1}}$=$\hat{\boldsymbol{a}}_{\boldsymbol{d2}}$=$\hat{\boldsymbol{a}}_{\boldsymbol{d3}}$) or ($\hat{\boldsymbol{b}}_{\boldsymbol{d1}}$=$\hat{\boldsymbol{b}}_{\boldsymbol{d2}}$=$\hat{\boldsymbol{b}}_{\boldsymbol{d3}}$) then,

$$\boldsymbol{c_{hd}} = \acute{\boldsymbol{c}}_{\boldsymbol{hd}} \tag{A21}$$

$$\boldsymbol{c_{hu}} = \boldsymbol{c_{hu}} + \hat{\boldsymbol{c}}_{\boldsymbol{bu}} \left(\frac{\overrightarrow{p_{u1}c_u} \cdot \boldsymbol{n_u}}{\overrightarrow{p_{u1}c_u} \cdot \boldsymbol{n_u} + \overrightarrow{p_{u1}c_{eu}} \cdot \boldsymbol{n_u}} \right) \tag{A22}$$

$$\boldsymbol{c_{hd}} = \boldsymbol{c_{hd}} + \hat{\boldsymbol{c}}_{\boldsymbol{bd}} \left(\frac{\overrightarrow{p_{d1}c_d} \cdot \boldsymbol{n_d}}{\overrightarrow{p_{d1}c_d} \cdot \boldsymbol{n_d} + \overrightarrow{p_{d1}c_{ed}} \cdot \boldsymbol{n_d}} \right) \tag{A23}$$

where $\boldsymbol{c_{hu}}$, $\acute{\boldsymbol{c}}_{\boldsymbol{hu}}$, $\boldsymbol{c_{hd}}$, and $\acute{\boldsymbol{c}}_{\boldsymbol{hd}}$ represent a number vector with three-dimensional coordinates. These are the starting points of the geometric vectors $\boldsymbol{c_{bru}}$ and $\boldsymbol{c_{brd}}$, and p_1, p_2, and p_3 are the three-dimensional coordinates of the structured water surface that defines the function of each water surface.

In the second step, using Snell's law, we can calculate $\boldsymbol{c_{bru}}$ and $\boldsymbol{c_{brd}}$ with the following equations.

$$\boldsymbol{c_{bru}} = \frac{1}{n_0} \{\boldsymbol{c_{biu}} + (e_u - m_u)\boldsymbol{n_u}\} \tag{A24}$$

$$e_u = -(\boldsymbol{c_{biu}} \cdot \boldsymbol{n_u}) \tag{A25}$$

$$m_u = \sqrt{n_0^2 + e_u^2 - 1} \tag{A26}$$

$$\boldsymbol{c_{brd}} = \frac{1}{n_0} \{\boldsymbol{c_{bid}} + (e_d - m_d)\boldsymbol{n_d}\} \tag{A27}$$

$$e_d = -(\boldsymbol{c_{bid}} \cdot \boldsymbol{n_d}) \tag{A28}$$

$$m_d = \sqrt{n_0^2 + e_d^2 - 1} \tag{A29}$$

$$n_0 = \frac{n_2}{n_1} \tag{A30}$$

n_1 and n_2 are $n_1 = 1.0$ and $n_2 = 1.33$, which represent the refractive indices of air and water, respectively.

Furthermore, in the third step, $\boldsymbol{b_u}$ and $\boldsymbol{b_d}$, which is the closest distance between $\boldsymbol{c_{bru}}$ and $\boldsymbol{c_{brd}}$, is calculated using the following equation.

$$\boldsymbol{b_u} = \boldsymbol{c_{hu}} + \boldsymbol{d_{u2}}\hat{\boldsymbol{c}}_{\boldsymbol{bru}} \tag{A31}$$

$$\boldsymbol{b_d} = \boldsymbol{c_{hd}} + \boldsymbol{d_{d2}}\hat{\boldsymbol{c}}_{\boldsymbol{brd}} \tag{A32}$$

$$\boldsymbol{d_{u2}} = \frac{(\hat{\boldsymbol{c}}_{\boldsymbol{bru}} \cdot \hat{\boldsymbol{c}}_{\boldsymbol{brd}})(\hat{\boldsymbol{c}}_{\boldsymbol{brd}} \cdot \boldsymbol{c_{hd}}\vec{\boldsymbol{c}}_{\boldsymbol{hu}}) - \hat{\boldsymbol{c}}_{\boldsymbol{bru}} \cdot \boldsymbol{c_{hd}}\vec{\boldsymbol{c}}_{\boldsymbol{hu}})}{1 - (\hat{\boldsymbol{c}}_{\boldsymbol{bru}} \cdot \hat{\boldsymbol{c}}_{\boldsymbol{brd}})(\hat{\boldsymbol{c}}_{\boldsymbol{bru}} \cdot \hat{\boldsymbol{c}}_{\boldsymbol{brd}})} \tag{A33}$$

$$\boldsymbol{d_{d2}} = \frac{(\hat{\boldsymbol{c}}_{\boldsymbol{bru}} \cdot \hat{\boldsymbol{c}}_{\boldsymbol{brd}})(\hat{\boldsymbol{c}}_{\boldsymbol{bru}} \cdot \boldsymbol{c_{hu}}\vec{\boldsymbol{c}}_{\boldsymbol{hd}}) - \hat{\boldsymbol{c}}_{\boldsymbol{brd}} \cdot \boldsymbol{c_{hu}}\vec{\boldsymbol{c}}_{\boldsymbol{hd}})}{1 - (\hat{\boldsymbol{c}}_{\boldsymbol{bru}} \cdot \hat{\boldsymbol{c}}_{\boldsymbol{brd}})(\hat{\boldsymbol{c}}_{\boldsymbol{bru}} \cdot \hat{\boldsymbol{c}}_{\boldsymbol{brd}})} \tag{A34}$$

$$\boldsymbol{b} = \frac{1}{2}(\boldsymbol{b_u} + \boldsymbol{b_d}) \tag{A35}$$

where $\boldsymbol{b_u}$, $\boldsymbol{b_d}$, and $\boldsymbol{b}$ are the number vectors whose components are the three-dimensional coordinates of the bed level, $\hat{\boldsymbol{b}}_{\boldsymbol{bru}}$, and $\hat{\boldsymbol{b}}_{\boldsymbol{brd}}$ represents the unit vectors $\boldsymbol{b_{bru}}$ and $\boldsymbol{b_{brd}}$.

In this method, the nearest points $\boldsymbol{b_u}$ and $\boldsymbol{b_d}$ for both the vectors were calculated. If the distance between the two points below the threshold values, which can be regarded as the distance between the two points, is set sufficiently, $\boldsymbol{b}$ is identified as an intersection for both the points.

From the aforementioned, the ST acquired the three-dimensional coordinates of the water surface and bed surface.

A3 Verification of the Measurement Accuracy

A31 Experiment Outline

The measurement accuracy of the water level and bed level of the ST for the alternate bars was verified using the following procedure. The channel that was used in the experiment was the same that was used in this study. In the movable bed experiment, in which the alternate bars were formed prior to the verification of the measurement accuracy, the channel slope was set to 1/200, the flow discharge was set to 1.7 L/s, and the riverbed material with an average particle size of 0.76 mm was used.

The bed shape that was measured consisted of a fixed bed was created by sprinkling thinly the cement powder. This bed shape is the alternate bars after 120 min when the water flow started from a flat floor. Immobilization with cement powder was carried out in a section that was 2 m in the central part of the waterway used in this experiment.

After confirming the adhesion of the cement powder, the water flow was restarted, and the water level and bed level were measured using the ST and point gauge. The measurement with the point gauge was set at intervals of 10 cm in the longitudinal direction and 2 cm in the transverse direction to capture the geometrical features of the alternate bars. The measurement section in the longitudinal direction was 200 cm for one wavelength of the alternate bar, which formed in the experimental channel. In addition, the measurement section in the transverse direction was 40 cm at the center of the channel. This was not affected by the reflection of the irradiation laser from the upper surface of the channel by the side wall. The ST measurement interval was set to 1 cm in the longitudinal and transverse directions.

A32 Measurement Results

Figure A6 shows the measurement results of the water surface and bed surface. In the figure, (a) and (b) are the shapes of the photographed water surface in the flow and the bed surface after drainage, and (c) and (d) display the water surface and bed surface levels that was measured by ST. In addition, (e) and (f) present the water surface and bed surface levels that were measured by the point gauge. Finally, (g) and (h) display the difference between the point gauge and ST for the water surface and bed surface levels.

As shown in Fig. A6, a wave sequence of the standing waves with a wavelength of approximately 7—10 cm is formed on the water surface in the water flow in the longitudinal direction. In addition, from (b), it can be observed that the alternate bars with a sedimentary height of approximately 0.5 cm are formed on the left bank side. It should be noted that the characteristic shape of the front edge and small undulations formed on the bars.

Next, by comparing (c), (d), (e), and (f) in the figure, the undulations of the high waves that are several centimeters in height cannot be reproduced at the water level and bed level at the measurement point intervals of the point gauge. Conversely, it can be reproduced in ST. For the measurement targets in this study, the wave with the shortest wavelength is the standing wave on the water surface. It can be observed that this wave can be reproduced well with a resolution of 1 cm, which can provide 10 measurement points in this wave. Figures A7 (a) and (b) show the histograms that were created from Fig. A6 (g) and (h), respectively. In this experiment, the water surface was constantly changing; it did not have a constant shape. Because a vertical fluctuation of approximately 2 mm was observed at the maximum point, the point gauge was measured to capture the center of the fluctuation range.

For this reason, Fig. A7 (a) shows the effect of the time fluctuations on the water surface. Therefore, even if there is no measurement error, it should be noted that the difference between the point gauge and the ST measurement value does not become 0.

By looking at the difference between ST and the point gauge, μ is -0.005 cm, σ is 0.063 cm for the water level measurement, μ is -0.203 cm, and σ is 0.093 cm when the bed level measurement is performed. When the measured value of the point gauge is used as the standard of the ST measurement accuracy, the measurement accuracy of the bed level is lower than the water level from the aforementioned results. However, it can be observed that the measurement accuracy is approximately 10 % of the maximum wave height of the alternate bars. From this, it can be concluded that this method has a sufficient measurement accuracy to measure alternate bars.

Appendix B Validity of the Pseudo-steady Flow Assumption that is applied to the Bars-Scale Riverbed Waves

This section describes the validity of the pseudo-steady flow assumption that is applied to the bars-scale riverbed waves. In this study, we introduced the assumption of a pseudo-steady flow when deriving the HPDE for the bed level z. This assumption is often introduced in stability analyses of bars-scale riverbed waves(Callander, 1969; Kuroki & Kishi, 1984). In the aforementioned stability analysis, it is assumed that the migration speed of the bed is sufficiently slower than the propagation velocity of the flow, and the flow can be treated as a pseudo-steady flow if the flow rate is constant. Based on this assumption, the stability analysis ignores the term of the time gradient in the continuity equation of flow and the equation of motion of flow among the governing equations that are used in the analysis. The aforementioned assumptions are considered to be valid. This is because the stability analysis explains the occurrence and developmental mechanisms of the alternate bars. However, to the best of our knowledge, whether the term of the time gradient of the flow can actually be ignored cannot be confirmed from the actual phenomenon. Therefore, we verified whether the term of the flow time gradient can be ignored with the ST measurement values and hydraulic analysis.

The aforementioned verification was performed by comparing the contributions of each term in the equation of motion for the flow.

$$\frac{1}{g}\frac{\partial u}{\partial t} + \frac{u}{g}\frac{\partial u}{\partial x} + \frac{\partial H}{\partial x} + I_{ex} = 0 \tag{B1}$$

H is the water level. As an explanation of the various physical quantities has already been mentioned, it is omitted here. The contribution of each term in the aforementioned equation was calculated for each ST measurement time, and the magnitudes were compared.

$\partial H/\partial x$ was obtained with the measured value of the water level of the ST. Other terms was obtained with the results of the hydraulic analysis, which is described in Section 4.1 in the main text. The time interval and spatial interval of the calculation were 1 min and 2 cm, which are the time resolutions and spatial resolutions of ST. The flow velocity and migration speed of the y component under the experimental conditions are 10^{-4} to 10^{1} of the x components at any location regardless of the developmental state of the alternate bars. For simplicity, the y component is ignored in this section.

Figure B1 shows the time change of the box-beard diagram that displays the contribution of each term. This figure shows the (a) local term, (b) advection term, (c) pressure term, and (d) friction term; they correspond to the order of each term

in Eq. (B1). By looking at the figure, although the (b) advection term, (c) pressure term, and (d) friction term dominate the flow at any time, it can be confirmed that (a) the local term can be ignored because the local term is smaller than the aforementioned three terms. Even if the advection term with the smallest contribution in (b),(c), and(d) is compared with the local term, the contribution of the local term is 10^{-4} to 10^{-2} of the (b) advection term. In addition, it can be observed that the local term is extremely small. From this, it is inferred that it is physically appropriate to ignore the time gradient of the flow in the alternate bars.

Appendix C Derivation of the Two-Dimensional Equation of the Water Surface Profile

Appendix C presents the derivation processes of the two-dimensional equation of the water surface profile to derive the HPDE for the bed level. The governing equations that were used for the derivation consist of the following continuous equations and the equations of motion. When deriving the equation, the flow can be treated as a pseudo-steady-state flow based on the verification results in Appendix B. Therefore, the following continuous equations and equations of motion are used for the derivation.

$$\frac{\partial [hu]}{\partial x} + \frac{\partial [hv]}{\partial y} = 0 \tag{C1}$$

$$\frac{u}{g}\frac{\partial u}{\partial x} + \frac{v}{g}\frac{\partial u}{\partial y} + \frac{\partial z}{\partial x} + \frac{\partial h}{\partial x} + I_{ex} = 0 \tag{C2}$$

$$\frac{u}{g}\frac{\partial v}{\partial x} + \frac{v}{g}\frac{\partial v}{\partial y} + \frac{\partial z}{\partial y} + \frac{\partial h}{\partial y} + I_{ey} = 0 \tag{C3}$$

As an explanation of the various physical quantities has already been mentioned, it is omitted here.

The derivation of $\partial h/\partial x$ is described as follows. First, applying the product rule to Eq. (C1) results in the following equation.

$$h\frac{\partial u}{\partial x} + u\frac{\partial h}{\partial x} + h\frac{\partial v}{\partial y} + v\frac{\partial h}{\partial y} = 0 \tag{C4}$$

Next, for the first and third terms on the left side of Eq. (C4),

$$u = \frac{1}{n}{I_{ex}}^{1/2}h^{2/3} \tag{C5}$$

$$v = \frac{1}{n}{I_{ey}}^{1/2}h^{2/3} \tag{C6}$$

$$\frac{\partial u}{\partial x} = \frac{\partial u}{\partial h}\frac{\partial h}{\partial x} + \frac{\partial u}{\partial I_{ex}}\frac{\partial I_{ex}}{\partial x} = \frac{2}{3}\frac{u}{h}\frac{\partial h}{\partial x} + \frac{1}{2}\frac{u}{I_{ex}}\frac{\partial I_{ex}}{\partial x} \tag{C7}$$

$$\frac{\partial v}{\partial y} = \frac{\partial v}{\partial h}\frac{\partial h}{\partial y} + \frac{\partial v}{\partial I_{ey}}\frac{\partial I_{ey}}{\partial y} = \frac{2}{3}\frac{v}{h}\frac{\partial h}{\partial y} + \frac{1}{2}\frac{v}{I_{ey}}\frac{\partial I_{ey}}{\partial y} \tag{C8}$$

After the differentiation of the composite function (Eq. (C7) and Eq. (C8)) using Manning's flow velocity formula (Eq. (C5), Eq. (C6)), substituting it into Eq. (C4), and rearranging $\partial h/\partial x$, the following equation is obtained.

$$\frac{\partial h}{\partial x} = -\frac{v}{u}\frac{\partial h}{\partial y} - \frac{3}{10}\frac{h}{I_{ex}}\frac{\partial I_{ex}}{\partial x} - \frac{3}{10}\frac{vh}{uI_{ey}}\frac{\partial I_{ey}}{\partial y} \tag{C9}$$

Next, after substituting Eq. (C7) and the following Eq. (C10) into the first and second terms of the equation of motion in the x direction for Eq. (C2),

$$\frac{\partial u}{\partial y} = \frac{\partial u}{\partial h}\frac{\partial h}{\partial y} + \frac{\partial u}{\partial I_{ex}}\frac{\partial I_{ex}}{\partial y} = \frac{2}{3}\frac{u}{h}\frac{\partial h}{\partial y} + \frac{1}{2}\frac{u}{I_{ex}}\frac{\partial I_{ex}}{\partial y} \tag{C10}$$

1043 the following equation is obtained. After substituting Eq. (C9), which was organized
1044 earlier into Eq. (C11),

$$\begin{aligned}\frac{3}{10}\frac{u^2}{gI_{ex}}\frac{\partial I_{ex}}{\partial x}-\frac{1}{5}\frac{uv}{gI_{ey}}\frac{\partial I_{ey}}{\partial y}+\frac{1}{2}\frac{uv}{gI_{ex}}\frac{\partial I_{ex}}{\partial y}+\frac{\partial z}{\partial x}\\ -\frac{v}{u}\frac{\partial h}{\partial y}-\frac{3}{10}\frac{h}{I_{ex}}\frac{\partial I_{ex}}{\partial x}-\frac{3}{10}\frac{vh}{uI_{ey}}\frac{\partial I_{ey}}{\partial y}+I_{ex}=0\end{aligned} \tag{C11}$$

1045

1046 The following equation can be obtained by rearranging $\partial h/\partial y$.

$$\begin{aligned}\frac{\partial h}{\partial y}=\frac{3}{10}\frac{u^3}{vgI_{ex}}\frac{\partial I_{ex}}{\partial x}-\frac{1}{5}\frac{u^2}{gI_{ey}}\frac{\partial I_{ey}}{\partial y}+\frac{1}{2}\frac{u^2}{gI_{ex}}\frac{\partial I_{ex}}{\partial y}\\ +\frac{u}{v}\frac{\partial z}{\partial x}-\frac{3}{10}\frac{uh}{vI_{ex}}\frac{\partial I_{ex}}{\partial x}-\frac{3}{10}\frac{h}{I_{ey}}\frac{\partial I_{ey}}{\partial y}+\frac{u}{v}I_{ex}\end{aligned} \tag{C12}$$

1047

1048 After substituting Eq. (C12) into Eq. (C9) and rearranging it, the following $\partial h/\partial x$
1049 is derived.

$$\begin{aligned}\frac{\partial h}{\partial x}=-\frac{\partial z}{\partial x}-I_{ex}-\frac{3}{10}\frac{u^2}{gI_{ex}}\frac{\partial I_{ex}}{\partial x}\\ +\frac{1}{5}\frac{uv}{gI_{ey}}\frac{\partial I_{ey}}{\partial y}-\frac{1}{2}\frac{uv}{gI_{ex}}\frac{\partial I_{ex}}{\partial y}\end{aligned} \tag{C13}$$

1050

1051 By rearranging $\partial h/\partial y$ using the same process as earlier, the following equation
1052 for $\partial h/\partial y$ is obtained.

$$\begin{aligned}\frac{\partial h}{\partial y}=-\frac{\partial z}{\partial y}-I_{ey}-\frac{3}{10}\frac{v^2}{gI_{ey}}\frac{\partial I_{ey}}{\partial y}\\ -\frac{1}{2}\frac{uv}{gI_{ey}}\frac{\partial I_{ey}}{\partial x}+\frac{1}{5}\frac{uv}{gI_{ex}}\frac{\partial I_{ex}}{\partial x}\end{aligned} \tag{C14}$$

1053

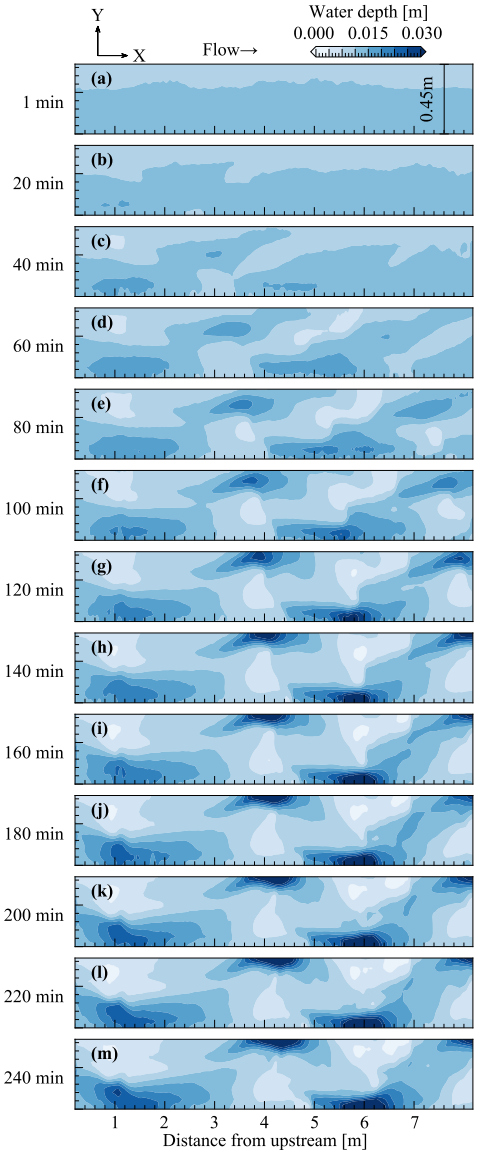

Figure 5. Temporal changes of the plan view for the observed water depth

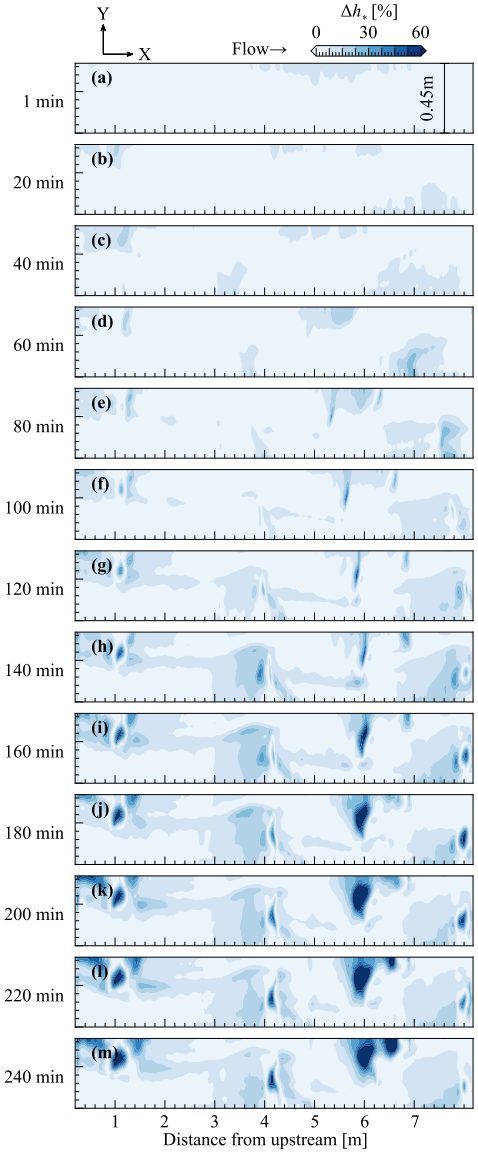

Figure 6. Difference between the measured value and the calculated value of the water depth that is made dimensionless by the measured value.

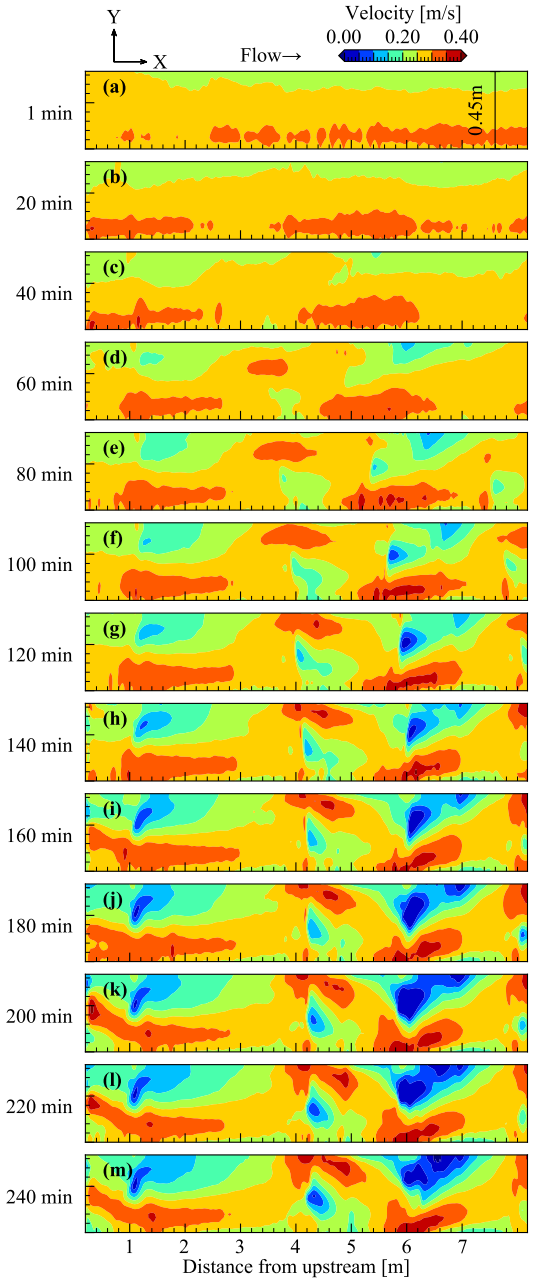

Figure 7. Temporal changes of the plan view for the calculated flow velocity

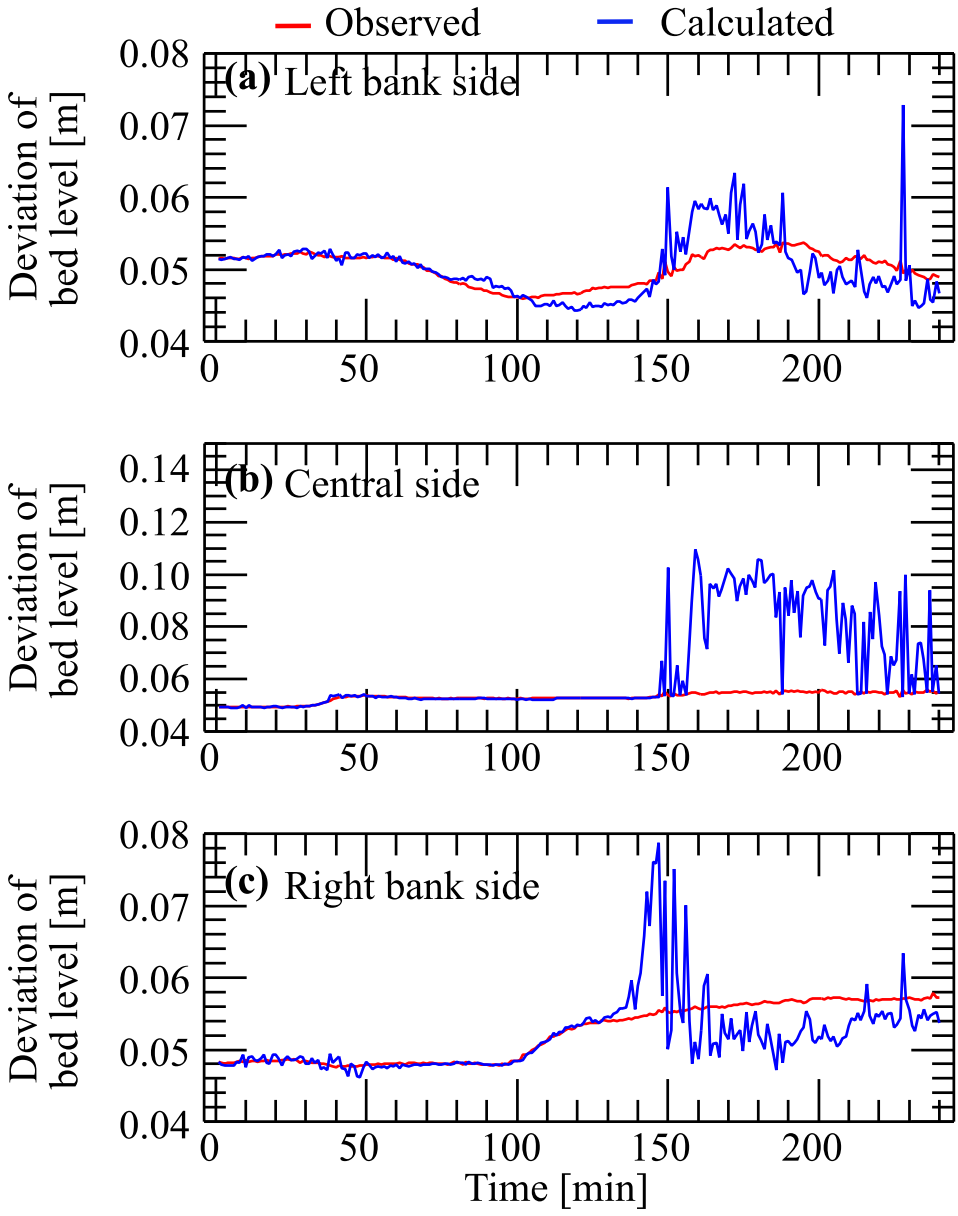

Figure 8. Bed-level time waveform. (a) Left bank side, (b) center, (c) right bank side

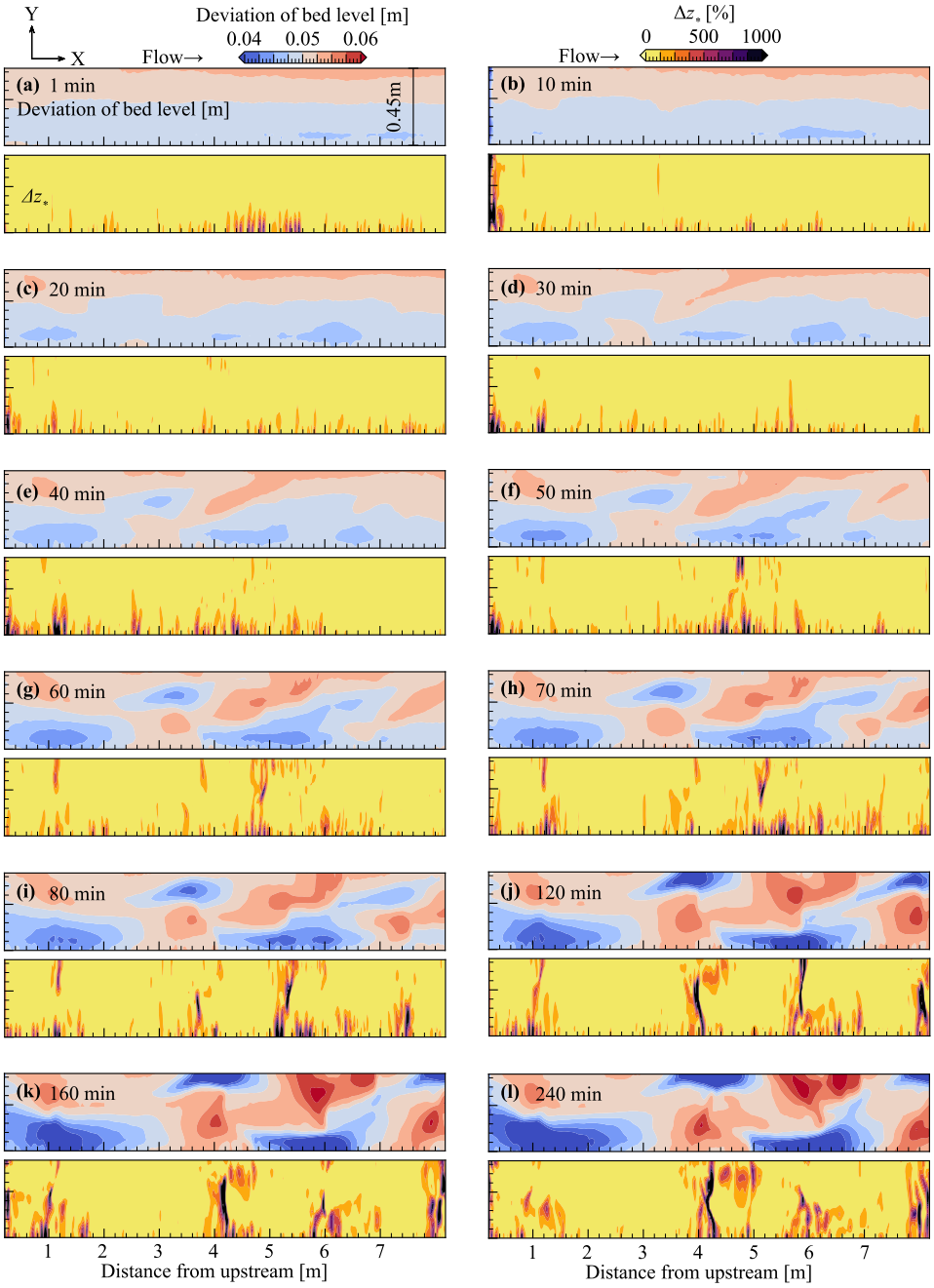

Figure 9. Temporal changes of the plan view for the observed bed topography and Δz_*

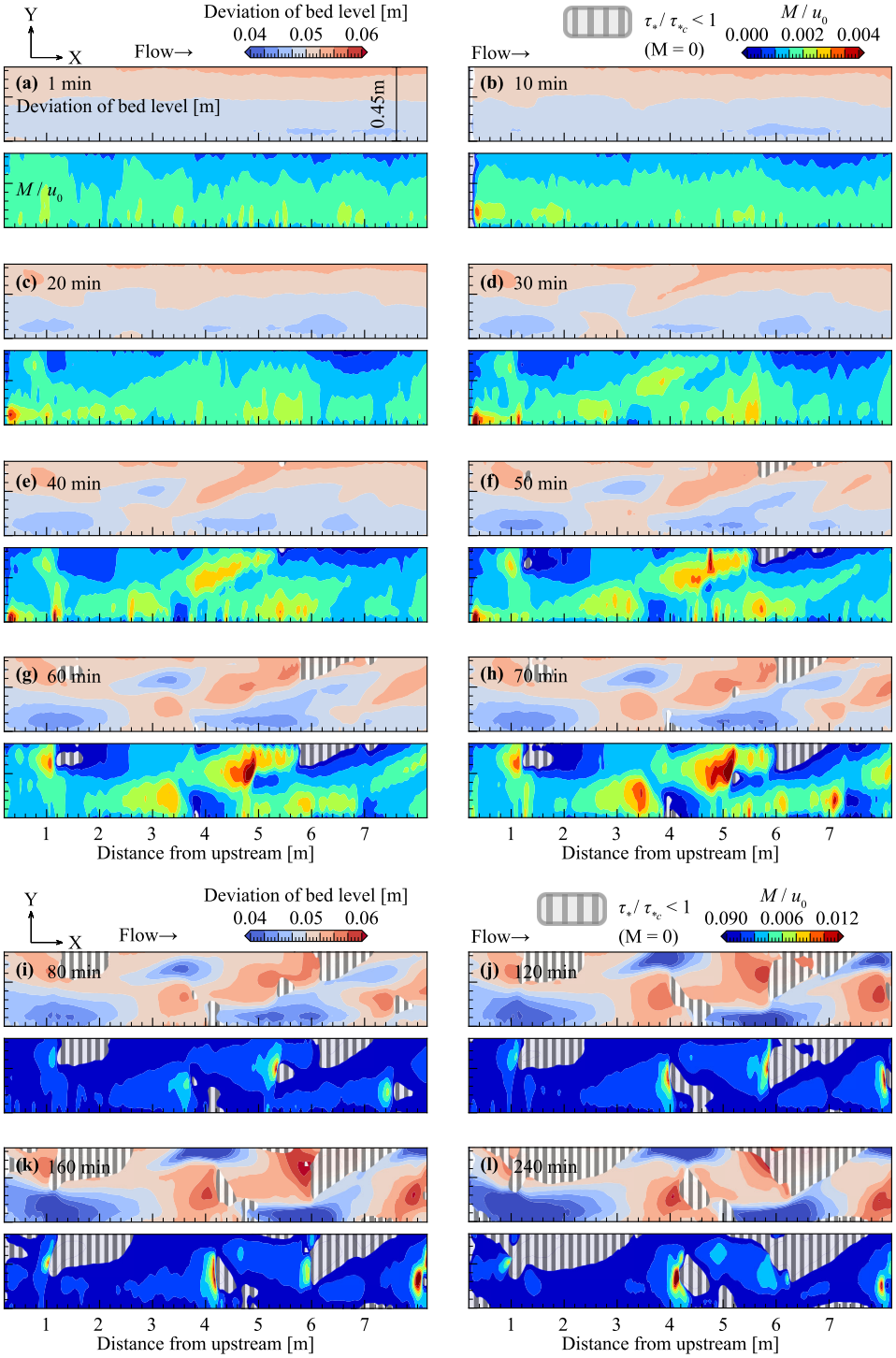

Figure 10. Temporal changes of the plan view for the observed bed topography and the calculated migrating speed

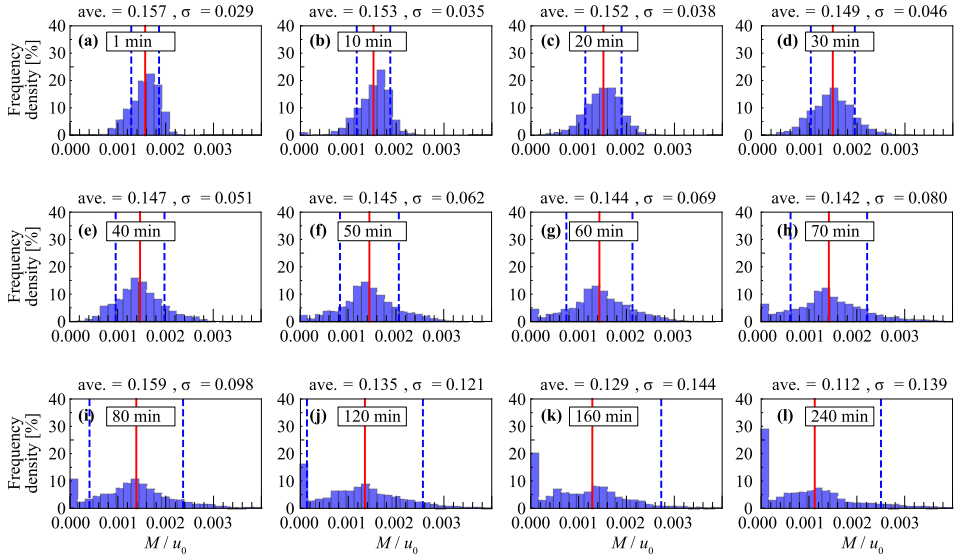

Figure 11. Histograms of the migrating speed

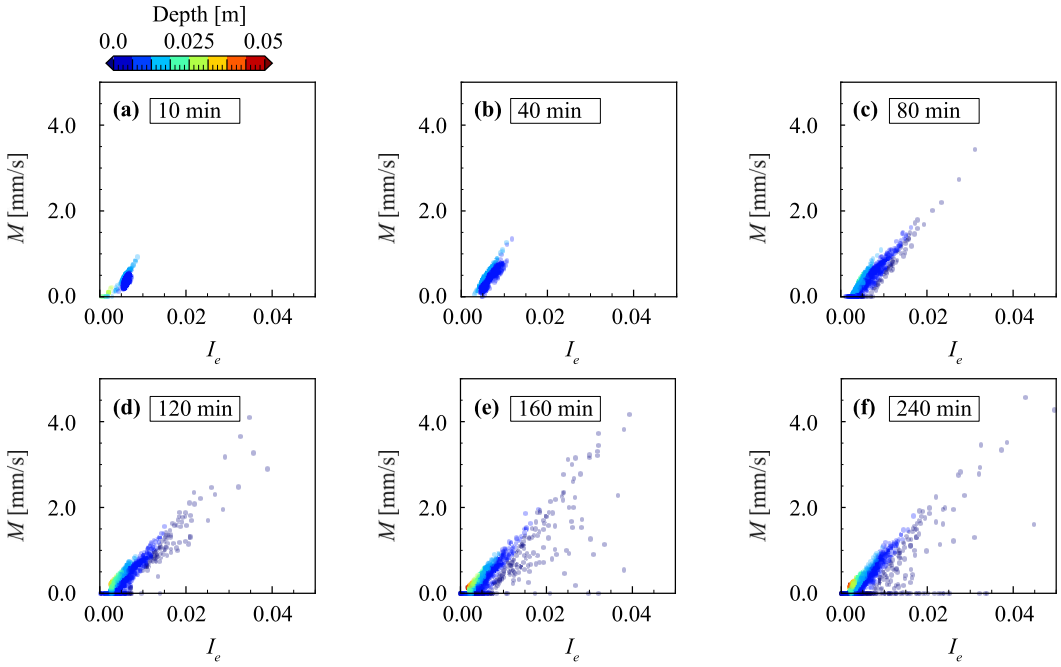

Figure 12. Relationship between the migrating speed, energy slope, and water depth

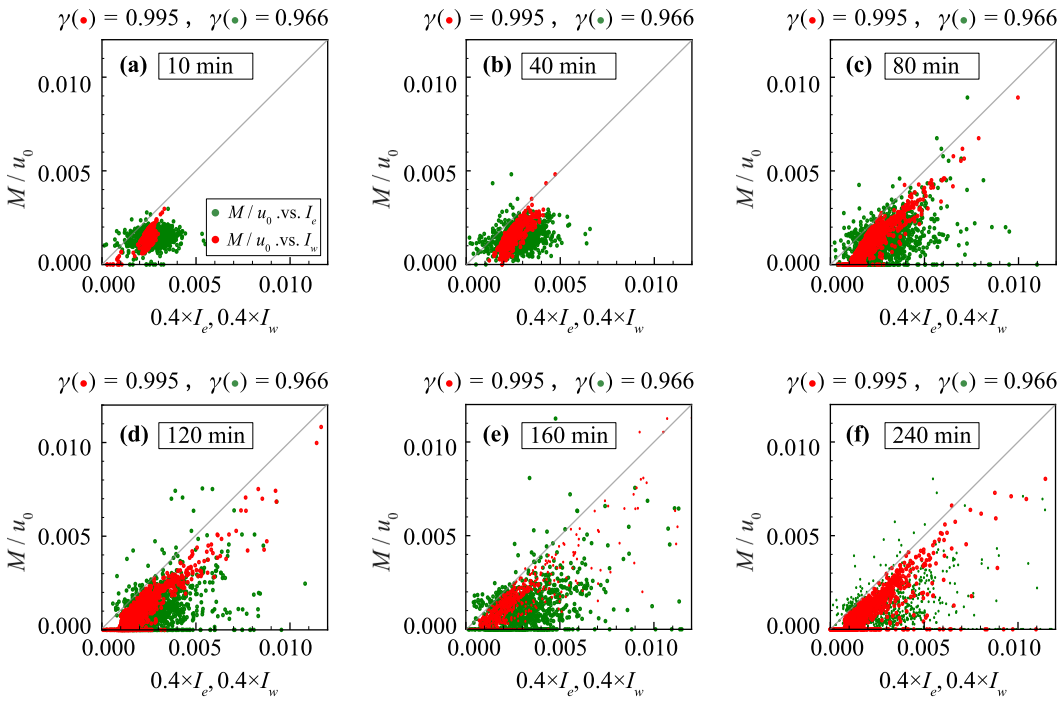

Figure 13. Relationship between the migrating speed, energy slope, and water surface slope

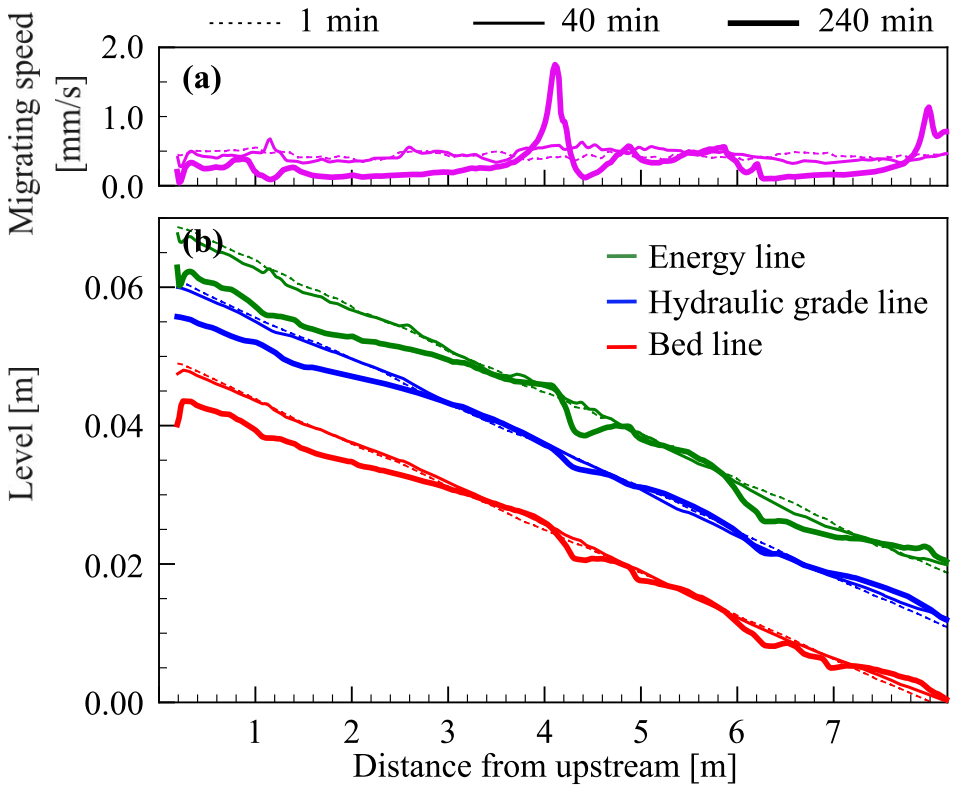

Figure 14. Longitudinal view of the (a) cross-sectional averaged migrating speed, (b) and cross-sectional averaged bed level

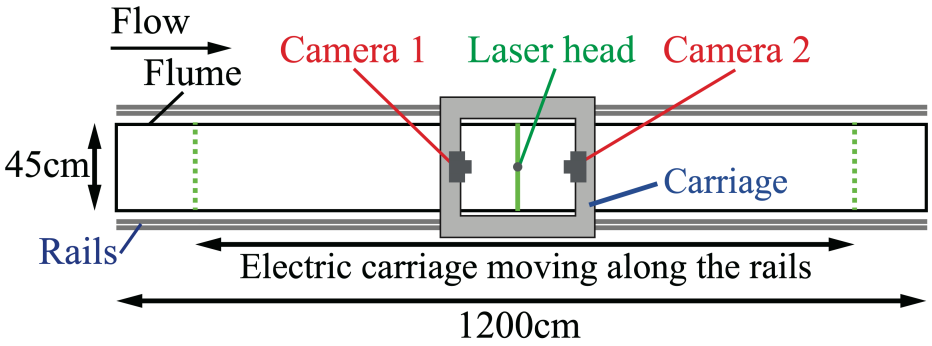

Figure A1. Overall plan view of the measurement device

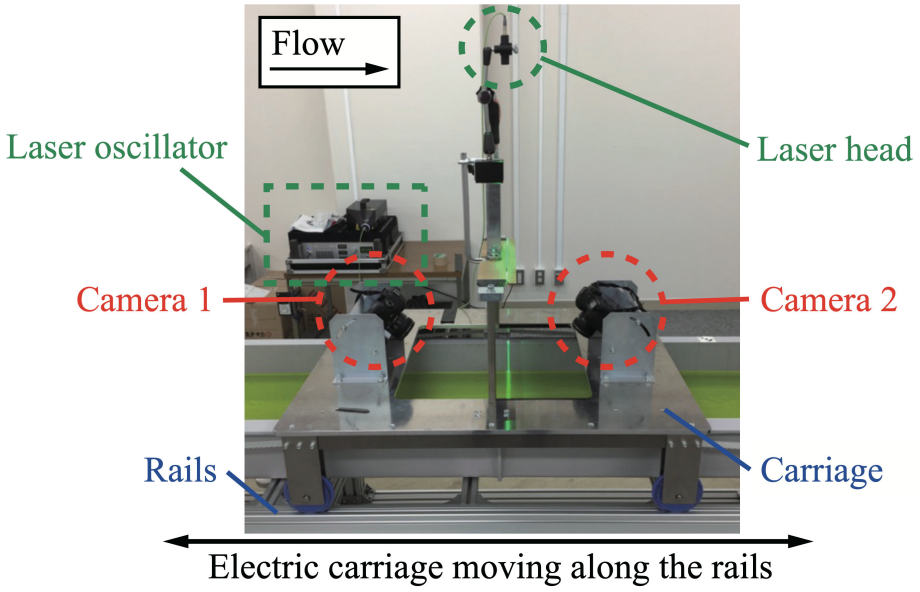

Figure A2. Equipment layout of the measurement equipment

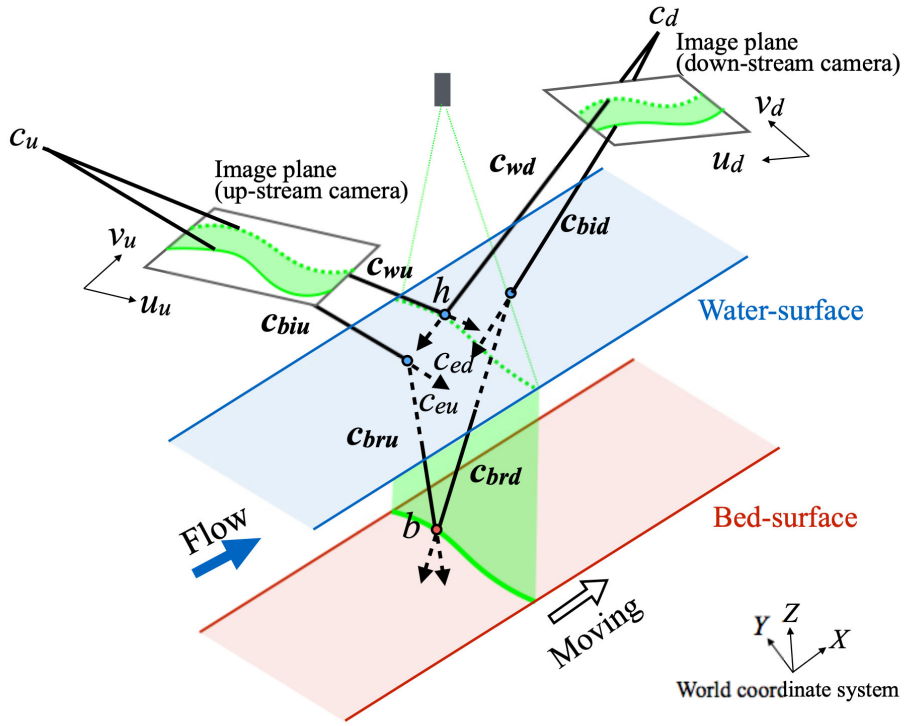

Figure A3. Outline of the measurement principle of the water surface and bed surface by triangulation

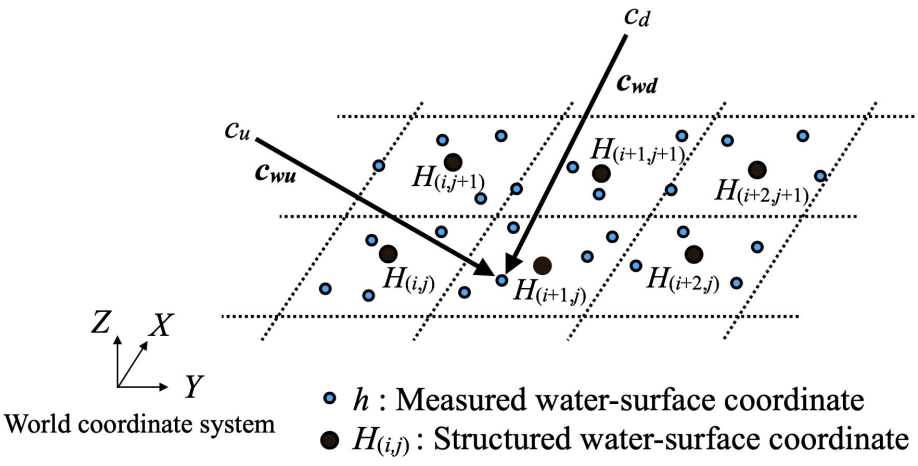

Figure A4. Relationship between $\boldsymbol{h}$ and H that is rearranged in a grid by triangulation

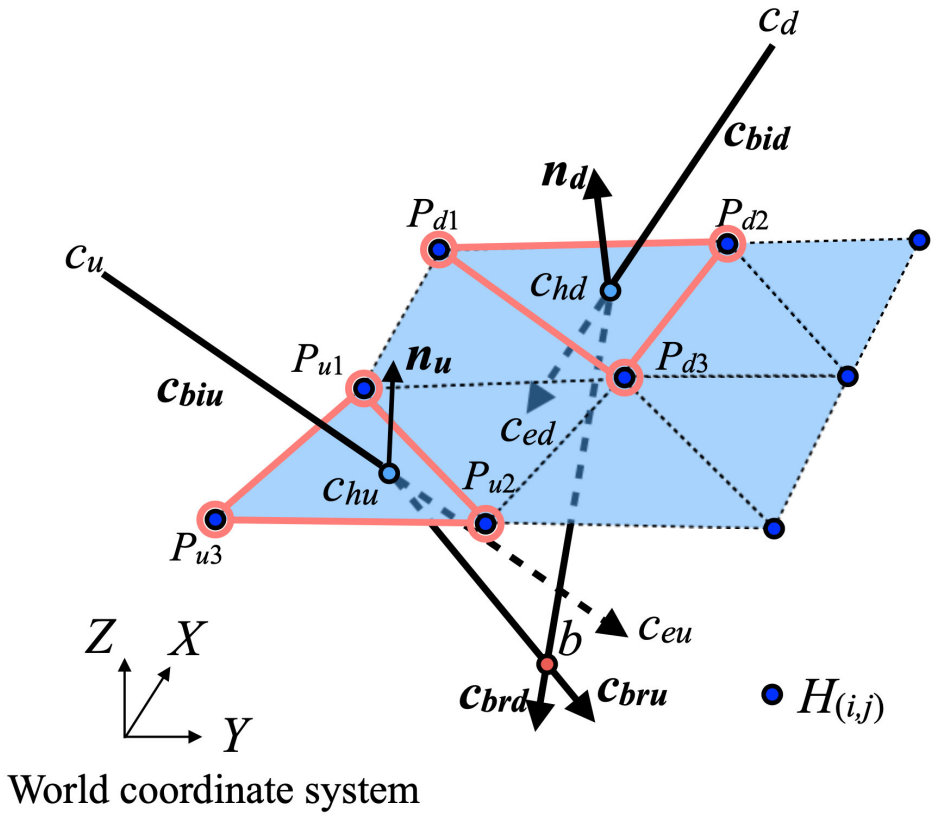

Figure A5. Outline of the bed surface measurement method while considering the refraction on the water surface

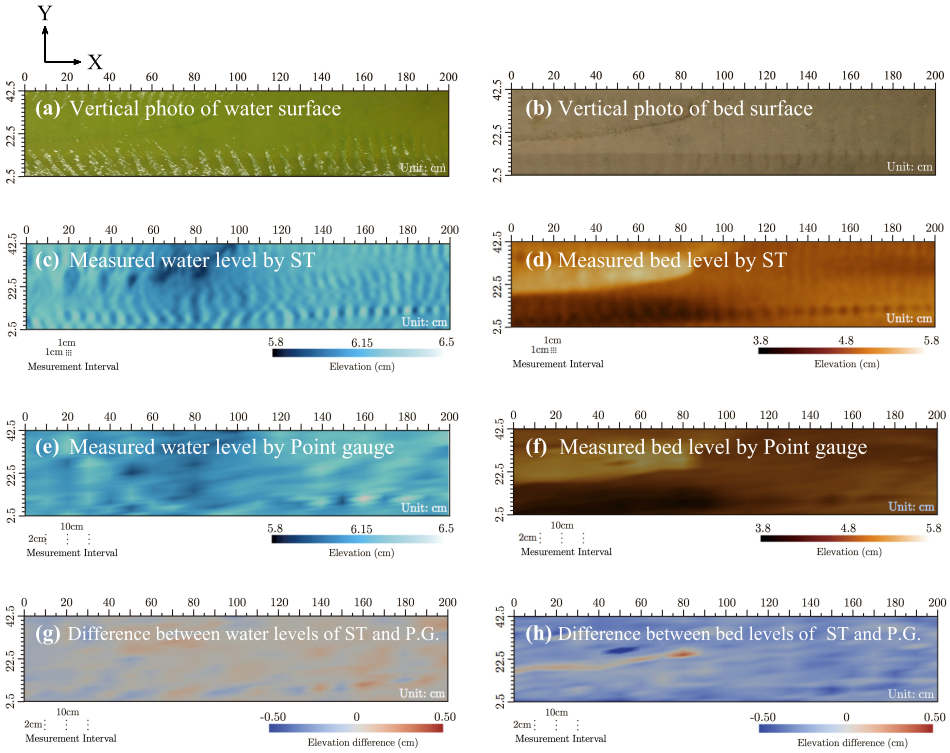

Figure A6. Measurement results of the water surface and bed surface

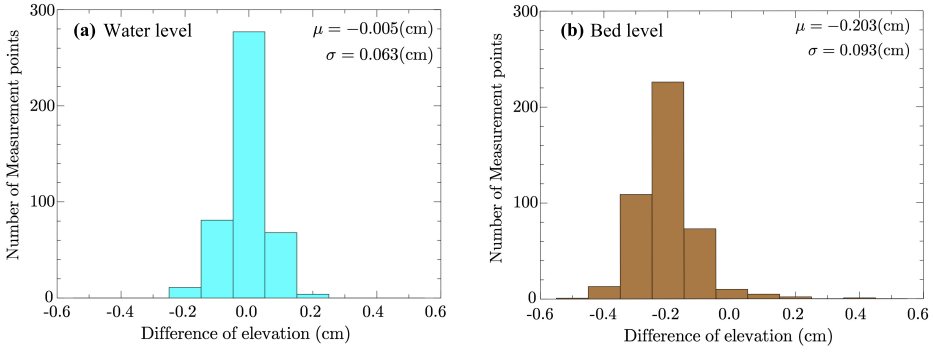

Figure A7. Histogram of the difference for the ST and point gauge measurements

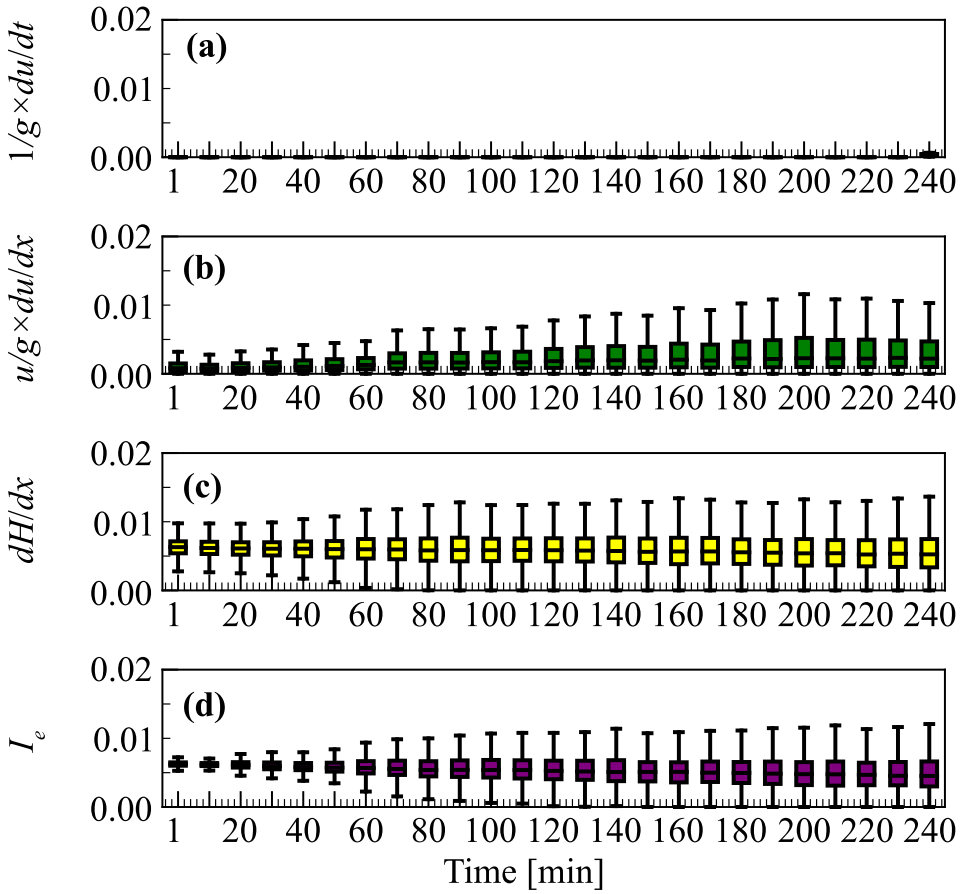

Figure B1. Temporal changes of the box plots for the (a) local term, (b) advection term, (c) pressure term, (d) and friction term